Faculdade de Engenharia da Universidade do Porto

System Identification and Evaluation for Hydrofoil Full State Feedback Control

Rui Sobreira Amorim de Sousa

Master Thesis

Mechanical Engineering Masters

Supervisor: Prof. António Mendes Lopes

Co-Supervisor at 4DC Tech: Dr. Ricardo Bencatel

Outubro 2022

Resumo

Este documento descreve o trabalho de Dissertação realizado para o Mestrado em Engenharia Mecânica, na especialização de Automação, na Universidade do Porto, em colaboração com a empresa 4DC Tech.

O tema versa a optimização do controlo em "full state feedback" de barcos com "hydrofoils", tendo em conta a sua dinâmica longitudinal e considerando 3 graus de liberdade (Avanço, Elevação e Inclinação), através de algoritmos para identificação de sistema e métricas que avaliem a sua eficácia e estabilidade. Este estudo advém de uma necessidade técnica e comercial, para o respetivo mercado.

Um resumo inicial aborda a evolução histórica de embarcações hidrófilas, desde os desenvolvimentos de Farcot às inovações realizadas por Bell. A física deste tipo de barcos, movidos a motor ou a vela, é explicada, abordando as propriedades das forças de arrasto e de sustentação com tecnologias "hydrofoils" específicas.

Descrevem-se também os pontos principais da teoria de controlo moderna, sendo apresentadas noções de espaços de estados e controlo em "full state feedback". Além disso são analisadas técnicas como o posicionamento de polos e LQR para demonstrar como a estabilidade e a eficácia de um sistema de feedback pode ser analisada ou otimizada.

Um dos primeiros passos para desenhar um controlador em espaço de estados, é o desenvolvimento de um modelo teórico que retrate o melhor possível a dinâmica do sistema. O modelo para o barco hidrófilo em questão é apresentado acompanhado pelas equações dinâmicas desenvolvidas para tal e pelos sistemas de coordenadas de referência.

Um modelo teórico pode ser útil como aproximação à dinâmica de um sistema, mas carece de informação relacionada com a influência de fenómenos não contabilizados nas equações. Para obter uma modelação realista, são utilizados algoritmos para identificação de sistemas a partir de dados recolhidos. Estes algoritmos são testados inicialmente em dados teóricos, para a verificação da sua utilidade e eficácia.

O processo para aplicação destes algoritmos em dados reais engloba: a linearização de ganhos não lineares em relação à velocidade do barco, tratamento de ruído e atrasos nos sinais, determinação da frequência de amostragem ideal e a produção do input necessário para a excitação das diferentes dinâmicas do sistema. Uma validação prática estava prevista, contudo, devido a logísticas do desenvolvimento do barco em questão, tal não foi possível a tempo da escrita desta dissertação. Como alternativa, os processos foram aplicados a dados de simulação para aprofundar o conhecimento da eficácia dos mesmos através das métricas referidas.

A estrutura do processo total é descrita para ser aplicada futuramente em dados recolhidos de testes práticos.

Abstract

This report presents the Master's degree dissertation in Mechanical Engineering, specialization in Automation, at the Faculty of Engineering of the University of Porto in collaboration with the company 4DC Tech.

The subject is the optimization of the full state feedback control of hydrofoil vessels in its longitudinal dynamics considering 3 degrees of freedom (Surge, Heave and Pitch) through system identification algorithms and metrics that evaluate its efficiency.

An initial summary regarding the hydrofoiling boats historical evolution is made, from the developments of Farcot to the innovations of Bell. The underlying physics of these types of sail and motorboats are explained mainly regarding the lift and drag properties of specific hydrofoil technology.

Following this, the modern control principles are introduced and a simple and short explanation is made to contextualize the readers of the control modern developments and the employment of state space equations and full-state feedback controllers. Furthermore, techniques like pole placement and LQR are demonstrated to show how feedback systems stability and performance can be analyzed and optimized.

Making an accurate model of a system's dynamics is one of the first steps in regulating it. The model for the hydrofoil boat under investigation is presented together with the equations that reflect its parameters and the coordinate systems used for reference.

A theoretical model can be an useful approximation to a system, however it will not describe its dynamics completely. To approximate this model to reality, system identification methods are used in order to identify a model's parameters using real data retrieved from the hydrofoil boat tests. Different system identification algorithms are tested in sample theoretical data to understand which ones are more reliable.

A process for applying these algorithms to real data is developed encompassing linearization of non linear gains in relation to boat's velocity, noise and delay, sampling frequency and input design. A practical implementation was predicted to be done, however that was not possible due to logistics problems with the hydrofoil in question. With that in mind, simulation data was analyzed and performance metrics adopted to assess the results.

Robustness and error metrics were investigated to be applied and give a better insight of the results.

A final process structure is summarized for future application of the sequence of processes discussed in the thesis for real data.

Agradecimentos

Passados 5 anos de faculdade, encontro-me a escrever a página final da minha dissertação, página esta que deixei para o fim para sentir realmente que o percurso estava a chegar ao fim e que agradeceria devidamente a quem fez parte deste.

Este caminho foi preenchido de obstáculos e desafios que me fizeram crescer e moldar na pessoa que me tornei hoje. Apesar de o meu conhecimento em diversas áreas ter crescido, sinto que o que mais mudou foi a maneira de olhar para o mundo, de aceitar argumentos de outros e perceber que apenas faço parte de um conjunto enorme de pessoas com objetivos semelhantes. É este conjunto de pessoas que começa agora a mudar o mundo.

Inicialmente agradecer aos meus pais e às minhas irmãs que são os pilares da minha estrutura e as cavalitas nas quais me apoio para conseguir ver o que vem à frente. São estes quem mais me ajudam e que estarão lá aconteça o que acontecer dia e noite, faça chuva ou faça sol.

Quero agradecer à restante família mais próxima, tios, sobrinhos, primos que também significam muito para mim e que, regularmente, me proporcionam visões diferentes do que é ser.

À minha namorada que desde o primeiro ano de faculdade me apoiou em todos os momentos, estudou comigo, festejou comigo e sofreu comigo. Resta-me retribuir o favor a ajudá-la a terminar o seu percurso, que ainda se encontra aberto, e contribuir para este tal como tanto contribuiu para mim.

Aos meus amigos. Essenciais para descomprimir e sorrir quando a vida não é tão fácil e quando nos encontramos mais sobrecarregados. A todos os que me desejaram felicidades e que nunca deixaram de estar nos meus sucessos e fracassos. Também agradecer aos amigos feitos na Faculdade que tantas horas partilhamos na Biblioteca, na Cantina, no Grill, na AE, e nos campos de Rugby Universitário.

Por último, a todos os professores, não só universitários, mas também do pré-escolar, do ensino básico e secundário até à faculdade. Houve muitas pessoas importantes na minha vida e frases, que até hoje, não esqueci e levarei para sempre comigo. São pequenos momentos que nos marcam e que nos fazem do que somos hoje. Ao Ricardo Bencantel (4DC Tech) que, apesar de ter um calendário apertado, sempre arranjou um tempo para me guiar e desbloquear quando me encontrava preso em alguma parte. Fica marcado o seu espírito de trabalho, inovação e resolução de desafios. Ao Professor António Mendes Lopes pela supervisionação da tese e apoio à estruturação e correção da mesma.

Obrigado a todos. Foi um grande percurso e sem vocês não estaria onde estou hoje. Que sejam felizes, que tenham o que merecem e que eu faça tudo o que for possível para retribuir e vos ajudar a atingir os vossos objetivos.

Rui Sobreira Amorim de Sousa

Contents

List of Figures

List of Tables

Introduction

The advent of ships capable of crossing seas and connecting the Earth's continents was one of the earliest disruptions in human mobility, enabling for the universal sharing of resources required for our development and progress. Since then, boats have continued to evolve, and today's fastest sailing boats hardly touch the sea. These vessels are known as hydrofoils and are characterized by its ability of cruising above the sea level. Hydrofoiling is gaining popularity as a technology that can improve boat travel efficiency (both motor and sail) by raising the hull above the water and minimizing drag energy losses.

Despite being far more energy efficient this technology requires sophisticated systems to control the vessel, assure stabilization and avoid major collisions. Due to our society's evolution and developments in the field of control we are capable of maintaining these boats in automatic control without the need of human intervention to keep them leveled and in the optimum traveling conditions.

However, like everything else, this can still be perfected and has margin to be improved upon, since the ocean challenges these hydrofoils with harsh conditions and a plethora of variables to evaluate and react to.

This thesis was developed alongside 4DC Tech, a Portuguese company that develops control systems for hydrofoil boats, both driven by motor and by sail. The control structure described in this report is based on the structure defined by 4DC Tech and their solutions applied to a variety of vessels. A solid theoretical base was already defined in the company's models, so the project proposed was centered in the practical model identification and optimization. The evaluation of control performance was key in the perception of the quality of this process. This required an initial research to discover the proper identification methods and their evaluation metrics, followed by the operations needed for their application in real data after processing.

1.1 Contextualization

Hydrofoiling is the practice of using foils or underwater wings (as it is named for airfoils) to generate enough lift and to raise a boat's hull, so that it can cruise without making contact with the water. By reducing the contact with the water, this technique enables a vessel to move with less drag, allowing it to move faster and more efficiently (energetically) when the right technology is used.

The first hydrofoil boat patent dates back to 1869, designed and built by the Parisian Inventor, Emmanuel Denis Farcot [32], despite being a rudimentary design it marked the beginning of the hydrofoiling era. For the purpose of this report, foil

and hydrofoil will have the same meaning, since they represent the same object.

Nowadays sailboats with foil based technology can achieve speeds 3.5 to 4 times the speed of the wind. The America's Cup [2], in which catamarans (2013 and 2017) and monohulls (2021) hydrofoils-driven sailboats compete at high speeds for the grand triumph, is one of the most prestigious sailing regattas. Luna Rossa's boat is shown in Figure 1.1 and was one of the highest performance sailing boats in 2021.

Figure 1.1: Luna Rossa in the America's Cup 2021 [7]

Besides racing, for our daily lives, this technology can reduce our purchasing costs and environmental impact. Around 80% of the cargo transported across our planet is moved in the ocean [43], so if we could optimize the energetic costs and consumption of this transportation, then our impact would reduce significantly. Even though the lift to velocity ratio generated by these hydrofoils is superior to that generated by airfoils, due to the higher density of the water, there is still much work to be done in order to be able to sustain the massive weights that cargo ships carry, with sufficient velocity, while controlling their stability and crossing the defying winds and waves of the outer ocean.

Even if we are not yet in the phase of implementing this technology on cargo and carrier ships, we have began developing control technologies that will advance hydrofoiling. Commercial and passenger vessels ranging in size from 10 to 30 meters are being developed by companies such as Mobyfly [34]. Seabubbles [48] has already launched prototypes that have proven to be successful in a variety of tests, outperforming current solutions for the Rotterdam's waterline in terms of economy, travel duration, and environmental friendliness [37]. As with any market disruption, the process must start small and gradually expand until it becomes second nature in our daily lives.

The tricky part for the evolution of these vessels is to ensure their stability against high oscillating and intensity winds, as well as big waves that tilt the boat in different axis, destabilizing the foil lift. Together, central and lateral foils provide the necessary lift and stabilization. Different types of controllers can be used to guarantee the control of the control surfaces. In this case a Full State Feedback controller [40] is the one of interest. A summary of the controller architecture and

implementation is provided in Section 2.4.1

Similarities can be found when comparing the control implemented in these boats to the ones in aircraft and, curiously, part of the developments made in this report, come from theory and practice implemented originally in aircrafts [3][25][20]. However, the level of precision in hydrofoils needs to be much higher since the margin of error fluctuates under 0.5 m, while in aircraft 50 m, at high altitudes, can be meaningless. The physics behind the lift and drag calculations related to the hydrofoils and airfoils is based on the same principles. These forces are computed by analyzing pressure differentials and how fluid velocity changes affect these gradients, as it is seen in Figure 1.2.

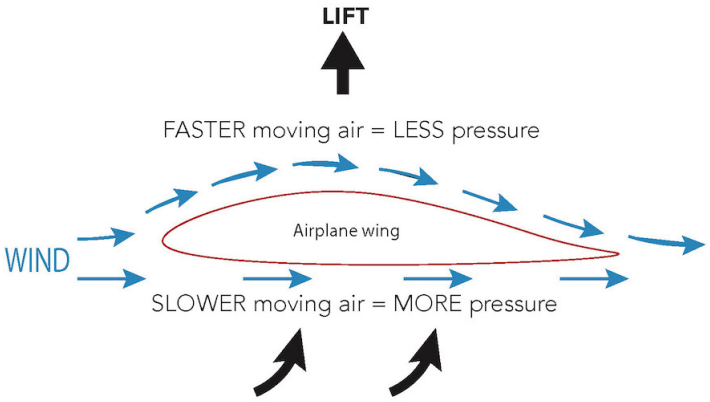

Figure 1.2: Wing pressure differential [50]

Finally, taking into account all the information stated above, it is clear that control optimization of hydrofoil vessels is not a direct approach. Several experiments need to be done and theory needs to be correlated with practice and real data. System identification has an important role in this aspect, since it can be possible to evaluate boat's dynamics through inputs and outputs gathered in real testing of the boats in various conditions. With this method we can compare the empirical values with the theoretical developed manually and assess, through different metrics, where the control parameters can be tuned and optimized in order to achieve more efficient and stable flight.

1.2 Motivation

It is significant to note that there are numerous variables to take into account when modeling such a complex system. Given that these boats go through challenging weather, including wind, waves, and temperature variations, it is clear that these environmental factors are perturbations and can have a significant impact on the stability of the entire control system. The correct control of the boat can be improved by exact models that accurately capture the dynamics of the system and take into account all noisy measurements.

The complexity along with the opportunity of innovation and to improve the way we tune a boat are the main drivers of this project. A lot of work has been done in the area of control, however it is not easy to come by with practical work

showing real data and proper exemplification of how to identify and optimize a MIMO (Multiple Input Multiple Output) closed-loop system. Mostly theoretical approaches are presented for system identification methods whilst work showing practical quantification and qualification of methods is scarce [11][59].

Reality is never a perfect reflection of our mathematical equations and approximations. Even if there are models that can achieve outstanding results, there is always a margin of error related to the inherent stochastic behaviour of a system. Through real data analysis, an approximation can be done and aligned with the previous theoretical computations achieving a equilibrium between both.

This report aims to discuss some of these topics and provide a tool to optimize system dynamics identification, as well as control performance analysis.

1.3 Report Outline

This work is structured as follows:

Chapter 2 describes the state-of-art. It discusses some of the work developed so far. This work is related to the developments in hydrofoil history, inherent physics, configurations and control in general.

Chapter 3 defines different models needed to apply the control theory.. The dynamics equations used to describe the system state-space matrices are presented.

Chapter 4 includes an overall theoretical look and application followed by the process developed for the application to real data of system identification methods. These are evaluated with identification performance metrics for various conditions.

Last but not least, control performance and stability metrics are shown in Chapter 5, followed by the conclusions and future works in Chapter 6.

State of the Art and Literature Revision

2.1 Historical Evolution

The history of hydrofoils is littered with significant turning points that collectively mark the boat industry's technological advancement. In this section, some of the important history will be discussed, followed by the technological principles that pushed this process forward.

After the first efforts by Emmanuel Denis Farcot, several patents were issued and hydrofoil technological potential rose. It was the Italian engineer, Enrico Forlanini, that designed and developed the first "serious" vessel in 1906, weighting 1202 kg with a 60 hp motor which could attain speeds of up to 69 km/h . It consisted in a ladder-like structure as shown in Figure 2.1. Forlainini, through his model experiments, proved that the lift was proportional to the speed squared. This meant that, as speed increased, less foil area was required. This area reduction was obtained with the ladder structure [32].

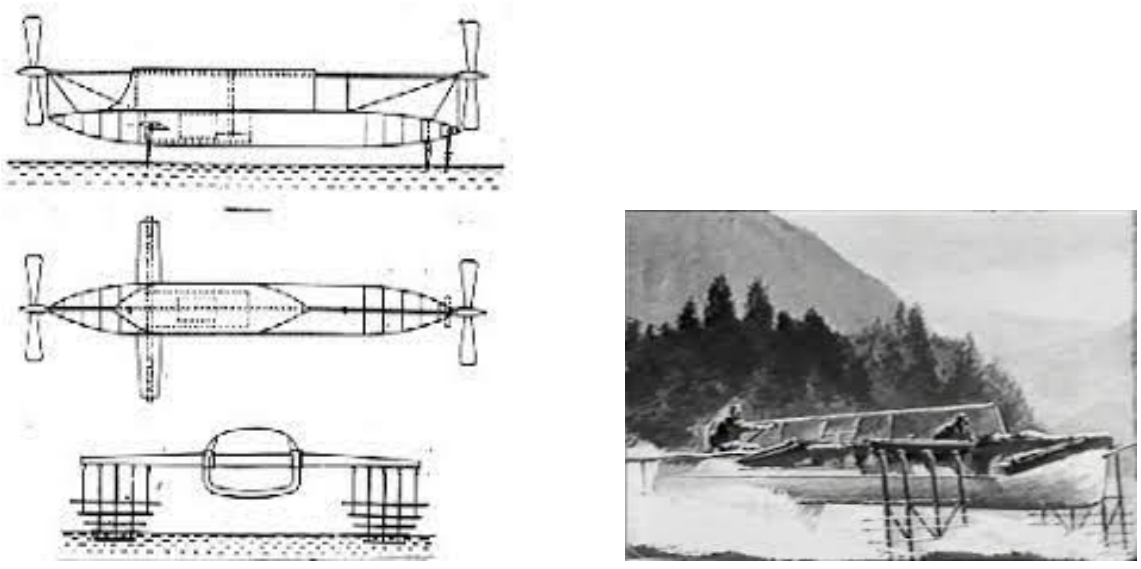

(a) Drawing schematic

(b) Prototype in action

Figure 2.1: Forlanini's hydrofoil representation with a ladder-like structure [32]

The next big step was done by Alexander Graham Bell (inventor of the telephone) and it was at this moment that hydrofoils got more publicity and awareness. Bell

denominated these ships as hydrodomes and his early prototypes resembled scaled-down airplanes. Only in 1918, with the assistance of Frederick Baldwin, did Bell develop the HD-4, the best hydrofoil at the time. The foils of this boat were arranged in such a way that it could continuously lift out of the water in a controlled and stable manner. This was referred as continuity or reefing, by Bell. The foils were spaced so that there was no vertical space between them. The lower part of one wing was the same height as the top end of the wing directly below it. The HD-4, in Figure 2.2, weighed 5 tons and was powered by two 350 hp engines reaching a speed of 114 km/h [51].

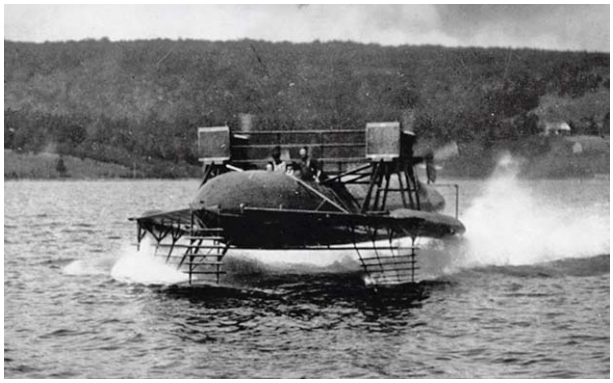

Figure 2.2: HD-4 [51]

The world of hydrofoil was calm between the HD-4 and 1927, with no important breakthroughs until Baron Von Schertel's inventions. Von Schertel experimented with hydrofoils in a variety of configurations, from fully submerged foils to v-shaped foils (details in Section 2.2), until he made the first trip demonstrating that hydrofoils can be used commercially by traveling in all weather conditions with seven people on board and achieving 55 km/h with a 50 hp motor. Schertel proceeded to work with the German navy during the World War 2 along with other important engineers, such as Tietjens, in a variety of hydrofoil projects, pushing the boundaries of this technology and paving the way for the next engineers [32].

Since then, numerous vessels were invented from large to small, fast to slow, for transportation of people, goods, from high mobility to high stabilization, propelled by sails or motors, with submerged or surface-piercing foils, and the list goes on [32].

The 1958 Canadian hydrofoil "BADDECK" was designed to demonstrate certain mechanical and structural attributes for use in other vessels. After the trials, it was determined that their foil system had failed and was insufficient, since the boat only remained stable in a limited range of foil angles. However, key conclusions were drawn from these experiments. Bell and his team's concepts had become outdated for heavier vessels and bigger waves, and using them as a foundation for getting the intended results was no longer productive. For surface-piercing foils, these ships should have a forward and aft (rear) foil, with the forward one acting as a trimming mechanism, allowing the main aft foil to react ahead of a wave. Also the main foil (aft) should be bigger. This arrangement was called "canard" and it was an important development for surface-piercing hydrofoil [32].

In 1955 the speed record for an hydrofoil was beaten for a speed of 144 km/h by the XCH-4 developed by the U.S. Navy, represented in Figure 2.3. This statistic is important because it encouraged the Navy to pursue the investment in this tech-

nology and forsee its potential. The record was broken again in 1963 by FRESH-1 an initiative pursued by Boeing and the NAVY with a speed of approximately 160 km/h [38].

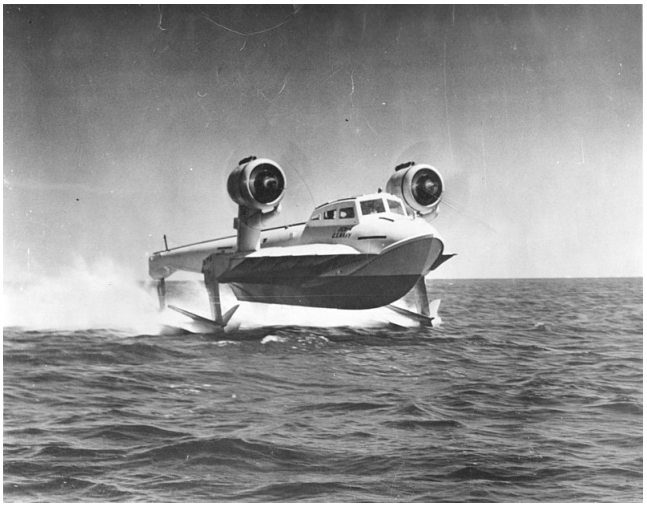

Figure 2.3: XCH-4 [32]

Various efforts have been made since then for the evolution of hydrofoils. Not always for the best reasons since there were projects with military interests, however some projects are intended to make the world a better place and to work in the sustainability of people and cargo transportation. These are the ones worth pursuing. Successful projects such as the Jetfoil [21] and Rodriquez Hydrofoils [12], have proven to be capable of transporting people (around 200 passengers) comfortably and efficiently, still with combustion engines and non-automatic control. Companies like Seabubbles [37] and Mobyfly [34] are pursuing the same objective but with renewable energy sources and automatic foiling control. These are in the prototype stage but have great future prospects. Hydrofoil technology and control systems were also pushed by the extremely agile and fast America's Cup sailboats that travel at speeds up to 100 km/h and have extremely fast responses in their control systems and maneuverability by riding in near unstable conditions. For more information on the history of hydrofoils John R. Meyer makes a really good job in his work [32].

2.2 Hydrofoils Arrangement and Inherent Physics

There are several possible arrangements and types of hydrofoils to establish in any hydrofoil boat. As it was shown in the historical part of the thesis, throughout the years the geometry and location of the hydrofoils changed abruptly as well as the materials and the treatments they are submitted to. A gathering of information related to this subject was made and it will be displayed briefly.

Hydrofoils are the main component that assures the boat's hull lift from the water providing it the main advantages of this systems. By uplifting the boat the drag forces are reduced significantly and the power needed to achieve the same velocities as a conventional boat is reduced. The net hydrodynamic force on the hydrofoil is given by the integration of the pressure and shear stress distribution over the entire

surface in contact with the fluid. Being F the resultant hydrodynamic force on the body, it can be calculated as in equation (2.1). In Figure 2.4a and 2.4b it is shown a more detailed version of Figure 1.2 and how lift and drag forces are generated, that is

$$F = -\int\int_S pndS + \int\int_S \tau kdS \tag{2.1}$$

where n and k are unit vectors, normal and tangent to the surface at a specific point, respectively, p and τ are the local and shear stress in the selected point. Finally dS is and infinitesimally small section of the wing [3].

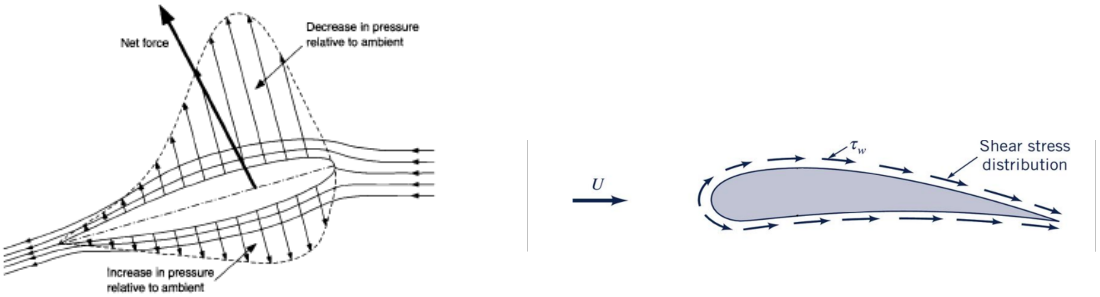

(a) Foil pressure distribution and forces [35]

(b) Shear stress distribution (adapted from [60])

Figure 2.4: Pressure and Sheer distribution

The net force represented can be divided into two different forces in the y and x direction, these being the lift and drag forces respectively, where they are inclined relative to the angle between the foil and the fluid free-stream, angle of attack. So the lift force is perpendicular to the free-stream whereas the drag force is parallel. In Figure 2.4b the free-stream is parallel to the foil and is represented by U, the angle of attack being 0°. In (2.2) and (2.3) these forces equations are represented and they are proportional to the square of the fluid free-stream velocity relative to the foil (U_0^2), to the fluid density (ρ), the projected area of the foil in relation to the direction of the respective force (S) and the respective coefficients ($C_L(\alpha)$, $C_D(\alpha)$) that represent complex dependencies and are determined experimentally in function of the foil angle of attack α [35]. These equations simplify integral calculations, because knowing the pressure and shear stresses for all areas of the wing in all conditions is considerably more complicated, therefore the lift and drag coefficients come in useful to simplify the computations [3], meaning

$$L = C_L(\alpha) \times S \times \rho \times \frac{U_0^2}{2} \tag{2.2}$$

$$D = C_D(\alpha) \times S \times \rho \times \frac{U_0^2}{2} \tag{2.3}$$

As it can be seen in Figure 2.5 the foil coefficient increases with the angle of attack until it achieves a stall position where the lift decreases abruptly inversely proportional to the drag. The stall condition occurs when the upper side of the foil is fully in the separation zone, the area where the fluid detaches from the surface of

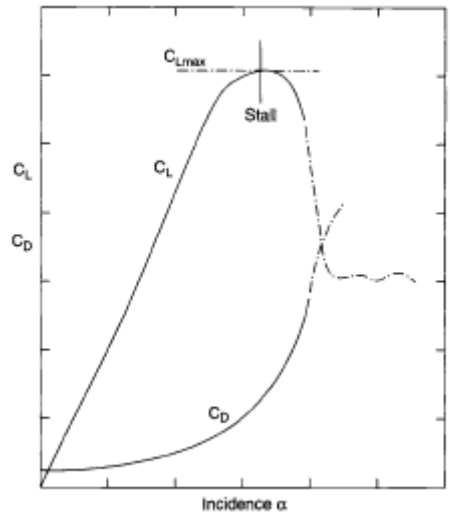

Figure 2.5: Lift and Drag coefficients in respect to α [35]

the foil and goes from laminar to turbulent [35]. In [3] an in depth description of the foil dynamics is done with accurate examples and explanations.

As the speed of the hydrofoil increases, the angle of attack of the foil can be reduced in order to maintain the lift force. The only scenario in which hydrofoils have more drag than conventional boats is before the takeoff where the whole structure of the foils is submerged and the hull is in contact with the water increasing the drag area, so it is important to keep the boat in the foiling condition, above the water, at all times. The control system is important to maintain this condition reacting to the past, current and predicted state of the system, commanding the different actuators.

Foils arrangement comes into play when designing the hydrofoil since different configurations are going to influence the boat stability, maneuverability, speed, etc. There are two main types of foil configurations: surface-piercing and fully-submerged, as it is seen in Figure 2.6. As the names indicate, the former refers to a configuration where the foils are partially submerged in the water whereas the latter defines the configuration where the foils are fully submerged.

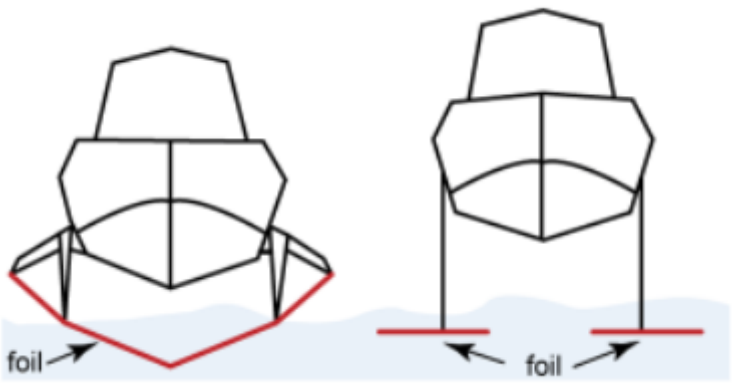

Figure 2.6: Surface-piercing foils (left) Submerged (right) [46]

The submerged part of the surface-piercing configuration is responsible for the lift of the boat's hull and as the speed increases the area of the foils submerged can be reduced and still lift the hydrofoil's weight due to the balance of the lift forces (equation (2.2)), that is why the foil is v-shaped and as the speed increases and the boat rises the foils get less submerged. This configuration can be defined as being self-stable since the foils automatically go deeper or higher as it is needed. It does not need automatic control, however, by doing this stabilization the boat is going to be oscillating and the foils are in constant interaction with the waves and the sea level oscillation, thus never being fully optimized and leveled. It can also be highly unstable when the boat rolls to turn. The ventilation in the transition area of the foil between the submerged and the non-submerged sections also generates a high induced drag, which is minimized by fully submerged foils.

Considering the fully-submerged configuration it can be deducted that the foils will need automatic control since they are always under water and the area of contact with the water remains the same. If the speed were to increase constantly the foils would fully come out of the water and the lift would be lost, causing the hull to crash and lose a big portion of its velocity. That is why it is needed a control system that varies the angle of attack of the foils, either through the entirety of the foil or partially through flaps, like an airplane, as it is shown in Figure 2.7 [32] [14] [46].

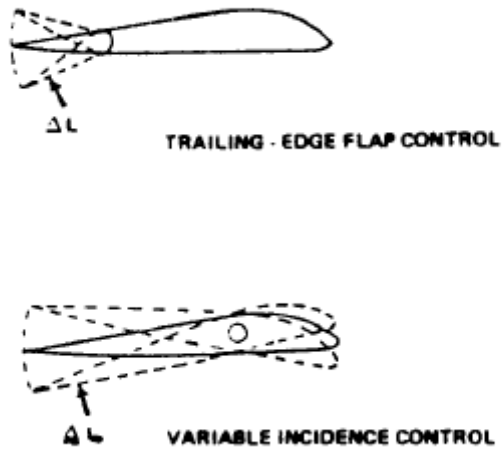

Figure 2.7: Entire foil angle variation (below), flap angle variation (above) [32]

Besides the foil configuration, these can also be located in different places of the hull and have different sizes according to the requirements. The most common arrangements are shown in Figure 2.8

The Canard and Conventional configurations are the ones that are more common in automatic control. The Canard configuration consists in one or two foils (if splitted) in the aft of the boat and one forward flap. The Conventional configuration consists in one or two flaps in the forward part of the boat and one flap in the rear. These configurations differ in the location of the bigger wing. Whether it is in front (Conventional) or behind (Canard) the *cg* (center of gravity of the boat), the bigger wing should be the closest to it, acting as an horizontal stabilizer. Splitted aft foils provide 1 more degree of freedom to command, since these flaps can be actuated individually, differentially or through an average between both. Essentially in this

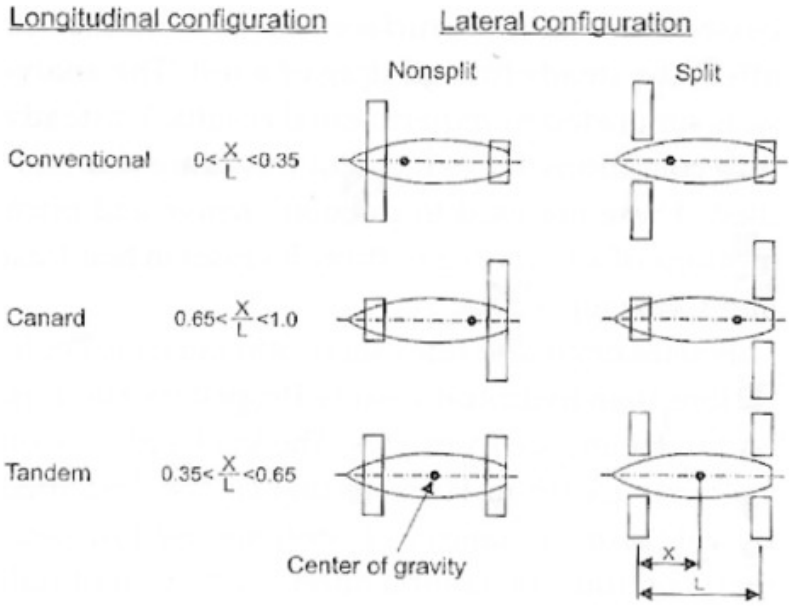

Figure 2.8: Foil Arrangements [32]

report the average aft flap command and forward flap command are going to be considered [9].

2.3 Hydrofoil Control

2.3.1 General Outline

Hydrofoil control can be a complex subject where multiple systems and forces interact with each other. The calculation of the hydrofoils dynamics is a subject by itself and is of great importance to construct an initial model and idea of how the system is supposed to behave and how it is necessary to be controlled.

Basically the whole physical dynamics can be divided in two: the actuator (servomotor) and the boat itself. Figure 2.9 describes properly how the commands interact and what happens in a control cycle for the Seabubbles prototype Sb4 [6].

The sensor system is composed by an ultrasound measuring the ride height of the boat in relation to the water whereas the IMU (inertial measurement unit) collects data through 3 gyroscope and 3 acceleration sensors. These provide information related to the different accelerations/velocities and the boat's inclination, in relation to the different axes. Both measurements are fused by an FNS (Foiling Navigation System) unit that estimates the necessary states by filtering/approximating the measurements to the most probable current state. Measurements usually are noisy and have inherent errors, that is why it is important to use an FNS unit. Also, other states cannot be directly measured or are not measured due to the lack of sensors or easiness of calculating through other measurements. The depth of the estimation and data collection is out of the scope of this report, although it is beneficial to have an idea of the process.

After the determination of the states, the controller is going to act according to the information presented. The controller can be of different types defined by the designer preferences and their advantages and disadvantages. The controller

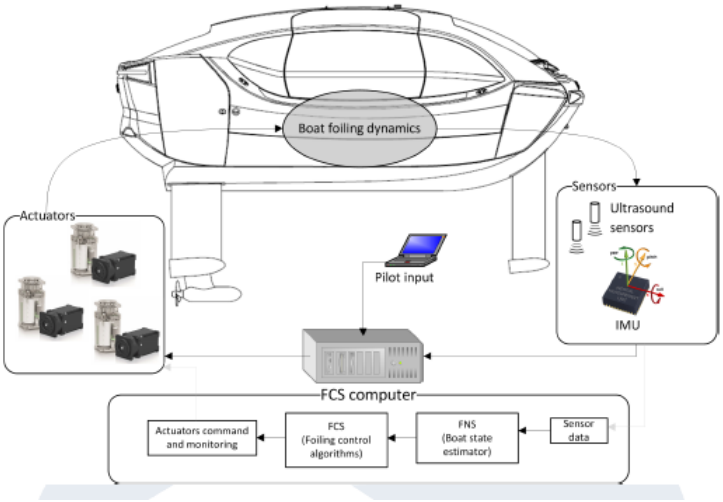

Figure 2.9: Foiling Control System subsystems [6]

objective is to compare its inputs (the current states of the system) and by firstly comparing them to a reference value compute a command for the actuators to act on the boat. The designer needs to define a gain matrix or a specific set of operations for the controller to apply according to the measurements performed. These gains/operations (depending on the controller) define the performance of the system in relation to the inputs it receives. If it is stable, fast or slow, overshoots or undershoots, among others.

The actuators will perform an action on the control surfaces of the boat and change its orientation. Depending on the boat dynamics and geometrical characteristics, the changes in the actuating surfaces are going to have a different effect in the state of the boat. These relations between the actuating surfaces and the actual changes in the boat's states are the parameters needed to determine and what makes this subject complicate.

2.3.2 FaRo Software

FaRo [15] is responsible for the design and implementation of navigation control systems for many different racing boats. Alongside with 4DC Tech, a partnership that began in 2014, they have developed software to perform automatic control for high performance hydrofoil boats such as the Luna Rossa's AC45s and Flying Nikka 60 for the America's Cup. For this report, FaRo's software has integrated the controller logic as well as a simulation algorithm developed by 4DC Tech. It was possible to input different excitations to the simulated actuators and generate data to be analyzed. As it is explained, more in depth, in Chapter 4.5.5 a function was created and implemented, in FaRo software, to develop predefined excitation through different input parameters.

Furthermore, it is possible to have access to simulations where the FCS (Foiling Control System) is turned off and have just the excitations providing the input to the boat. Through this actions an overview of the boat's open-loop dynamics is illustrated.

2.4 Control Theory

Several questions need to be made and answered before anyone tries to implement any sort of control technique in order to manipulate some variables to achieve a desired performance or condition in a given element. In the case of this report the system is an hydrofoil boat, more precisely the Seabubbles SB4 and it is characterized by a mathematical model, a set of equations that represent the dynamics of the system as precisely as possible. This mathematical model is not unique for a system due to the possibility of different interpretations and simplifications decided by the brain behind the model development, since we can not represent reality 100% accurately. To do so we use differential equations that represent how a system will vary according to specific inputs and the correlation of the its inherent variables [40].

The control part of the system appears when we decide to generate actions through the manipulation of different actuators (motors, pistons, etc.) and influence its internal variables or states through the correlation of the actuators variations and these states alteration.

With that being said control theory can be divided into two categories: classical and modern.

Classical control methods are based on Fourier and Laplace transforms and these methods are common for SISO systems (Single Input Single Output). Also these use controllers known as PID (Proportional–Integral–Derivative) that include the three operations that are represented in the name - multiplication by a constant, integration and derivation. Other forms of the PID controller appear when one or more operations are neglected and the controller ends up being simply proportional or proportional-integral for example [41]. For MIMO systems with a higher order differential equation the representation in state-space is simpler.

2.4.1 Modern Control (State-Space)

Control systems have been evolving throughout the years and along with this evolution comes complexity. MIMO systems have become more common and the control techniques to handle them as well. The way we are deciding to represent our MIMO system is by structuring it into state space equations, organizing this equations into matrices that represent its dynamics. For more complex systems is usual to use this state space equations due to its simplicity and computing velocity. This technique is applicable to linear or nonlinear, time varying or time invariant systems through a time and frequency domain approach. Classic control theory contrasts with this since it is only applicable to SISO, linear and time-invariant systems, thorough a complex frequency domain approach [40].

If we consider a simple mechanical system consisting on a mass, a spring and a damper, as represented in Figure 2.10, we can derive its mechanical equations in the Newtonian way, equaling the external net forces to the sum of the system's objects momentum change, that is

$$u = m\ddot{y} + b\dot{y} + ky \tag{2.4}$$

Immediately, we can distinguish the different terms that compose this equation. On the left-hand side there is the external force applied, and on the right-hand

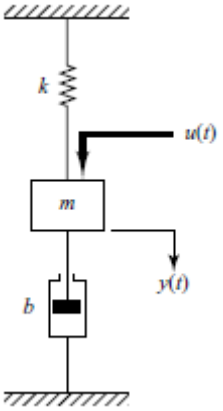

Figure 2.10: Dumped Spring Mass mechanical system (adapted from [40])

side the terms related to the kinetic energy, the potential energy, and the energy dissipation. Also, there are 3 possible states that can be identified $(y, \dot{y}, \ddot{y})$, however only two of these states are needed since the acceleration can be found through position and velocity. With that being said there are a minimum of 2 states needed to describe the system at any given moment knowing the system parameters. Thus, this is a second order system and we can define its states as:

$$x(t) = \begin{bmatrix} x_1(t) \\ x_2(t) \end{bmatrix} = \begin{bmatrix} y(t) \\ \dot{y}(t) \end{bmatrix}$$

The state-space continuous time representation of a linear, time-invariant deterministic system can be represented as:

$$\dot{x} = Ax(t) + Bu(t) \qquad x(0) = x_0 \tag{2.5}$$
$$y = Cx(t) + Du(t) \tag{2.6}$$

where A is the system matrix that represents the internal relation between the system variables and parameters, B is the control matrix that represents the relation of the states to the inputs, $u(t)$ and C and D are the output matrices. Matrix C is used to determine the desired outputs function of the states (usually is an identity matrix) and D is used to bypass inputs directly to the output (usually a zeros matrix). In the end, the output is basically the calculation of the states in relation to the past states and current input/command. By applying the state-space equations to (2.4) it is trivial to understand the meaning of each component.

We can now consider $\dot{x}$ as the derivative of states $x_1(t)$ and $x_2(t)$:

$$\dot{x} = \begin{bmatrix} \dot{x}_1(t) \\ \dot{x}_2(t) \end{bmatrix} = \begin{bmatrix} \dot{y}(t) \\ \ddot{y}(t) \end{bmatrix} \tag{2.7}$$

Then, as $\dot{x}_1(t) = x_2(t)$ and transforming equation (2.4) to matrix form we get the final state space representation as

$$\begin{bmatrix} \dot{x}_1(t) \\ \dot{x}_2(t) \end{bmatrix} = \begin{bmatrix} 0 & 1 \\ -\frac{k}{m} & -\frac{b}{m} \end{bmatrix} \begin{bmatrix} x_1(t) \\ x_2(t) \end{bmatrix} + \begin{bmatrix} 0 \\ \frac{1}{m} \end{bmatrix} u \tag{2.8}$$

$$y = \begin{bmatrix} 1 & 0 \end{bmatrix} \begin{bmatrix} x_1(t) \\ x_2(t) \end{bmatrix} \tag{2.9}$$

where

$$A = \begin{bmatrix} 0 & 1 \\ -\frac{k}{m} & -\frac{b}{m} \end{bmatrix}, B = \begin{bmatrix} 0 \\ \frac{1}{m} \end{bmatrix}, C = \begin{bmatrix} 1 & 0 \end{bmatrix}, D = 0 \tag{2.10}$$

There can be multiple state space representations for the same system by considering different states, basis, outputs and inputs.

Now that the equations that describe the system are defined, we can proceed to the implementation of the control. Figure 2.11 depicts a Full State Feedback for a linear, time-invariant system block diagram. Besides the state space equations defined above, there is also a gain matrix K that defines how the control is going to act upon the system. In the Section 2.4.2 it is going to be explained how it is possible to manipulate the gains of the K matrix in order to change how the system is commanded.

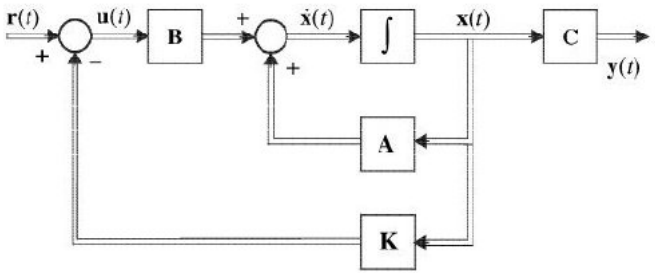

Figure 2.11: Full State feedback system block diagram [29]

When developing a full state feedback controller of the system there are two important notions to take into consideration: controllability and observability. These are related to the capability of the actuators to influence the system and the existence of sensors that measure the necessary states, respectively.

A system is controllable if it can output control signals that allow a system the reach any desired state in a limited amount of time. The controllability of a system is evaluated through the matrix in (2.11) and can only be assumed controllable if C is of $rank(n)$ being n the order of the system [22].

$$C = [A \quad AB \quad ..... \quad A^{n-1} \quad B] \tag{2.11}$$

A system is observable if all the states can be known through the system outputs. It is important to note that the states of the system need to be known for very discrete time parcels, this usually requires high sample frequency that depends on high quality sensors. The system states can be obtained directly (through sensors) or indirectly through calculations involving other measurements. If matrix (2.12) is of $rank(n)$ the system can be considered observable:

$$O = \begin{bmatrix} C \\ CA \\ . \\ . \\ . \\ CA^{n-1} \end{bmatrix} \tag{2.12}$$

For more information on this section the references [40] [53] [13] provide good guidance.

2.4.2 Pole Placement

From looking at the diagram in Figure 2.11 and considering the state space equations, it is possible to start deriving the closed-loop matrices of the system. Replacing in (2.5) $u(t)$ by $(r(t) - Kx(t))$ we get,

$$\dot{x} = Ax(t) + B(r(t) - Kx(t)) \tag{2.13}$$

and

$$\dot{x} = (A - BK)x(t) + Br(t) \tag{2.14}$$

where $(A-BK)$ represents the closed-loop A matrix or A_{cl}. Determining the eigenvalues of A_{cl} through its determinant, $\det(A_{cl} - \lambda I)$=0 we can analyze the poles of the system, and with the variation of K get different responses. Considering a transformation of the system we obtain,

$$\dot{Z} = \tilde{A_{cl}} Z \tag{2.15}$$

where $\tilde{A_{cl}}$ represents the eigenvalues of A_{cl} in its diagonal. In this representation, $\dot{Z}$ is affected only by its own state, since $\tilde{A_{cl}}$ is a diagonal matrix. Representing $\dot{Z}$ this way presents a simplification to the solution of Z, where it is in the form of

$$Z_n = Ce^{\lambda t} \tag{2.16}$$

It is now possible to simply plot the response of a state to a given initial condition for $t = 0$, given by C. By changing the value λ the response is changed. A simple way of analysing this problem is to plot the Real and Imaginary axis and plot the values for λ. The way λ is placed shows how oscillatory and how the energy is going to be dissipated in the state response. The first major factor to avoid are real positive poles, because they originate unstable responses. Also poles that are "too negative" can be unfeasible due to the system incapability of performing to those speeds. Imaginary poles originate oscillating responses and, according to the real part, they can exponentially grow or decay. Figure 2.12 depicts how the location of the closed-loop poles of the system can affect its response.

The method described is intuitive, and the easiest way to understand how the simple manipulation of a gain matrix can change how a system reacts to different changes. However, when systems get more complex, pole placement can be tricky. This because it is hard to understand how different poles are going to interact with each other and originate a final response. Other methods can be applied, such as the LQR.

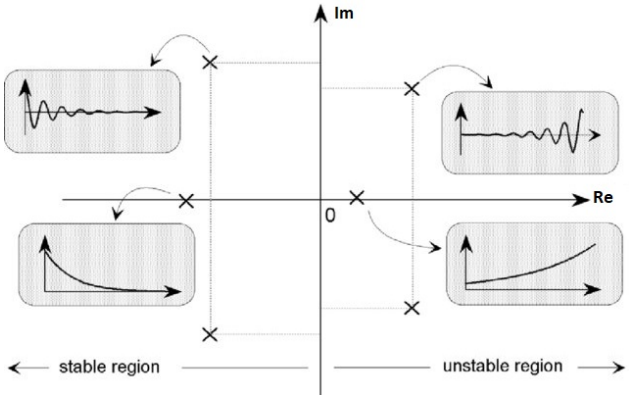

Figure 2.12: Poles effect on system response [26]

2.4.3 LQR

The LQR method is more intuitive in order to find an optimal solution for the controller gains of a specific problem. In this it is useful to think of it as finding the optimal solution for a given problem, where the user decides the weight/relevance he attributes to the controller effort and to the performance of the controller. When more energy, money and resources in general are used, it is normal that the controller performs better. Needless to say that infinite resources are not in play and that at some time the amount of money/energy invested does not correspond linearly to the increase in performance obtained.

The optimization process for the LQR method uses from base a cost function:

$$J = \int_0^\infty x(t)^\intercal Q x(t) + u(t)^\intercal R u(t) dt \tag{2.17}$$

with

$$K = R^{-1} B^\intercal S \tag{2.18}$$

where K is the gain matrix determined, Q is an $n \times n$ weight matrix associated with the states, being n the order of the system, R is an $m \times m$ weight matrix associated with the inputs, being m the number of inputs and S is the solution for the algebraic Riccati equation. Since Q is a positive semi-definite matrix and R is a positive definite matrix, the integral is always going to be a positive value.

The end goal is to minimize the cost function respecting the state space equations (2.5). It is clear that the more we increase Q or R coefficients the more importance is being given to each part of the equation. For high performance, increase Q and for low effort, increase R.

The mathematical development to solve these equations can be seen in [39], that develops a method to solve the Ricatti equation (2.18) for the optimum values of K. More than one set of solutions is given by these equations, so it is important to select the one that ensures the system stability.

All-in-all LQR can be a useful method for practical and fast tuning of a controller, by adjusting the values from the Q and R matrices according to the given results [27]. This is the method used for the determination of the gain matrices in this scope.

Models

3.1 Coordinate System

The overall dynamics of a boat can be represented in the 6 DOF axes referential, consisting of 3 linear and 3 rotation motions. Also two coordinate systems are defined, one with its origin in the ocean surface, representing the "World" or "Global" referential, and one in the center of gravity of the boat, moving analogous with the boat along its coordinates in the Global referential. Figure 3.1 depicts the boat coordinates in its referential system and its nautical motion denominations, where Xs aligns with the forward direction of movement, Zs to the vertical motion pointing to the earth and Ys to the starboard (right) side of the ship. X,Y and Z represent the global axes that are attributed arbitrarily to a point of reference [55].

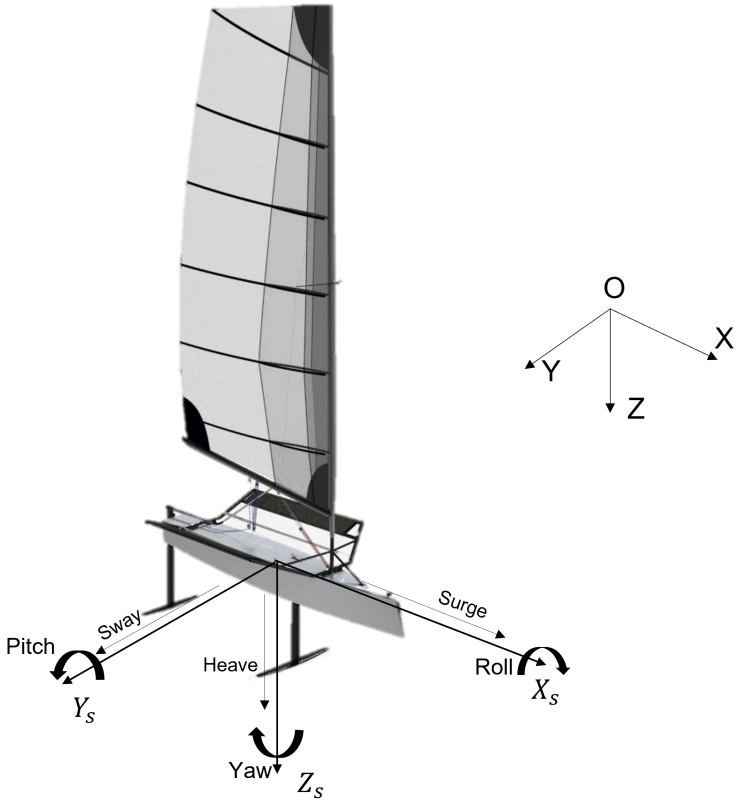

Figure 3.1: 6 DOF coordinate system

The control of the boat's orientation in the Euler angles, is going to be done through the different actuating surfaces present in the system. These can be the

aft and forward foils, the rudder, the thruster and any other auxiliary surfaces implemented by the designers. This control for the hydrofoils is usually divided in 3DOF (longitudinal dynamics) or the 6DOF (longitudinal + transversal dynamics). In Figure 3.1 the different DOF are depicted.

The linear motions along the axis Xs,Ys and Zs are the surge, heave and sway, respectively, whereas the rotational motions are the roll, pitch and yaw, respectively. For the purpose of this thesis only the 3DOF coordinate system is going to be considered [5].

Also to control these motions 2 actuating surfaces are commanded: the forward flap, and the average between the port (left side of the boat) and the starboard aft (rear) flaps.

3.2 Dynamics Model

As it was said previously, before trying to identify a system, it is important to have a notion of what results are expected. This theoretical approach had already be done for the hydrofoil being worked on and, in this section, the models being used are described.

This preliminary model was developed for the Seabubbles SBH2V1 boats in this report [6].

Initially 3 DOF are going to be considered, and these are related with the longitudinal dynamics of the boat. These are, the longitudinal speed(along the Xs axis), the pitch (rotation along the Ys Axis) and the heave (vertical displacement along the Zs axis). Ultimately, for the dynamics of the 3DOF, 5 states are needed to fully describe the longitudinal dynamics. These are included in the state vector in (3.1). $\dot{x}$, is given by vector (3.2):

$$x = \begin{bmatrix} \Delta V & \omega & q & \Delta Z & \Delta\theta \end{bmatrix}^\intercal \tag{3.1}$$

$$\dot{x} = \begin{bmatrix} a_{X_S} & \dot{\omega} & \dot{q} & \omega & q \end{bmatrix}^\intercal \tag{3.2}$$

where ΔV is the longitudinal speed variation, a_{X_S} the longitudinal speed acceleration, ω is the vertical rate, $\dot{\omega}$ the vertical acceleration, q is the pitch rate, $\dot{q}$ the pitch acceleration, ΔZ is the vertical displacement and $\Delta\theta$ is the pitch variation.

The inputs considered are the forward flap actuation (FF) and the average aft flaps average command (FA) represented in (3.3):

$$u = \begin{bmatrix} \delta_{FF} & \delta_{FA} \end{bmatrix}^\intercal \tag{3.3}$$

After determining the dimensions of the state and input vectors, it is possible to assume the dimensions of matrix A and B, as being 5×5 and 5×2, respectively.Their parameters are represented in equations (3.4) and (3.5). Important to notice that these matrices only refer to the dynamics of the boat, other two matrices are needed for the actuator dynamics, to be coupled to the boat's dynamics. However, the actuators dynamics are simpler and well known since they have been tested by the manufacturers several of times, in order to improve the accuracy of their parameters determination. When integrated with the boat, there could be a change in the dynamics of the servomotor, but they are less significant than the changes that have an effect in the boat's dynamic matrices.

$$A = \begin{bmatrix} X_V & X_W & X_q & X_Z & X_\theta \\ Z_V & Z_W & Z_q & Z_Z & Z_\theta \\ M_V & M_W & M_q & M_Z & M_\theta \\ 0 & 1 & 0 & 0 & 0 \\ 0 & 0 & 1 & 0 & 0 \end{bmatrix} \tag{3.4}$$

$$B = \begin{bmatrix} X_{\delta_{FF}} & X_{\delta_{FA}} \\ Z_{\delta_{FF}} & Z_{\delta_{FA}} \\ M_{\delta_{FF}} & M_{\delta_{FA}} \\ 0 & 0 \\ 0 & 0 \end{bmatrix} \tag{3.5}$$

The dynamics parameters are represented in equations (3.6) to (3.24) and the control parameters in equations (3.25) to (3.30) [6]. Looking at matrix A it is possible to realize where the ones come from representing the equalities existing between $\dot{x}$ and x. In $\dot{x}$ the last two rows represent the height rate and pitch rate, respectively, that also exist in the x vector, in this case, being the represented by the second and third rows. This originates equalities represented by ones and null relations represented by zeros.

$$X_V = -\frac{2SQ}{mV} C_{D,V} \tag{3.6}$$

$$X_W = -\frac{SQ}{mV}(C_{D,\alpha_{WF}} + C_{D,\alpha_{WA}}) \approx \frac{X_\theta}{V} \tag{3.7}$$

$$X_q = \frac{SQ}{mV}(C_{D,\alpha_{W_F}} x_{WF} + C_{D,\alpha_{WA}} x_{WA}) - X_V \frac{z_{WF} + z_{WA}}{2} \tag{3.8}$$

$$X_Z = \frac{SQ}{m\bar{b}} C_{D,h} \tag{3.9}$$

$$X_\theta = -\frac{SQ}{m} C_{D,\theta} \approx -\frac{SQ}{m}(C_{D,\alpha_{WF}} + C_{D,\alpha_{WA}}) \tag{3.10}$$

$$Z_V = -\frac{2SQ}{mV} C_{L,V} \approx -\frac{2g}{V} \tag{3.11}$$

$$Z_W = -\frac{SQ}{mV}(C_{L,\alpha_{WF}} + C_{L,\alpha_{WA}}) \approx \frac{Z_\theta}{V} \tag{3.12}$$

$$Z_q = \frac{SQ}{mV}(C_{L,\alpha_{W_F}} x_{WF} + C_{L,\alpha_{WA}} x_{WA}) - Z_V \frac{z_{WF} + z_{WA}}{2} \tag{3.13}$$

$$Z_Z = -\frac{SQ}{m\bar{b}} C_{L,h} \tag{3.14}$$

$$Z_\theta = -\frac{SQ}{m} C_{L,\theta} \approx -\frac{SQ}{m}(C_{L,\alpha_{WF}} + C_{L,\alpha_{WA}}) \tag{3.15}$$

$$M_V = -\frac{2S\bar{c}Q}{I_{yy}V} C_{m,V} \tag{3.16}$$

$$M_W = -\frac{S\bar{c}Q}{I_{yy}V}(C_{m,\alpha_{WF}} + C_{m,\alpha_{WA}}) \approx \frac{M_\theta}{V} \tag{3.17}$$

$$M_q = -\frac{S\bar{c}Q}{I_{yy}V}(C_{m,\alpha_{W_F}} x_{WF} + C_{m,\alpha_{WA}} x_{WA}) + M_V \frac{z_{WF} + z_{WA}}{2} \tag{3.18}$$

$$M_Z = -\frac{S\bar{c}Q}{I_{yy}\bar{b}} C_{m,h} \tag{3.19}$$

$$M_\theta = -\frac{S\bar{c}Q}{I_{yy}} C_{m,\theta} \approx -\frac{S\bar{c}Q}{I_{yy}}(C_{m,\alpha_{WF}} + C_{m,\alpha_{WA}}) \tag{3.20}$$

$$Q = \frac{\rho V^2}{2} \tag{3.21}$$

$$L = C_L SQ \tag{3.22}$$

$$D = C_D SQ \tag{3.23}$$

$$M = C_m S\bar{c}Q \tag{3.24}$$

$$X_{\delta_{FF}} = -\frac{SQ}{m} C_{D,\delta_{FF}} \tag{3.25}$$

$$X_{\delta_{FA}} = -\frac{SQ}{m} C_{D,\delta_{FA}} \tag{3.26}$$

$$Z_{\delta_{FF}} = -\frac{SQ}{m} C_{L,\delta_{FF}} \tag{3.27}$$

$$Z_{\delta_{FA}} = -\frac{SQ}{m} C_{L,\delta_{FA}} \tag{3.28}$$

$$M_{\delta_{FF}} = -\frac{S\bar{c}Q}{I_{yy}} C_{m,\delta_{FF}} \tag{3.29}$$

$$M_{\delta_{FA}} = -\frac{S\bar{c}Q}{I_{yy}} C_{m,\delta_{FA}} \tag{3.30}$$

where m is the boat mass and I_{yy} is the inertia moment around the boat lateral axis. g is the gravity acceleration. $C_{\#,\alpha_{WF}}$ and $C_{\#,\alpha_{WA}}$ are the coefficients for the angle of attack of the whole forward and aft foil wings, respectively. x_{WF},x_{WA}, z_{WF} and z_{WA} are the x and z coordinates of the forward and aft foils hydrodynamic centers with respect to the center of gravity. L and D are the lift and drag forces, respectively given by (3.19), (3.20) and $C_{\#}$ the corresponding coefficients, M is the pitch moment and C_m the corresponding coefficient, S is the total foils area projected on the horizontal plane. $\bar{b}$ and $\bar{c}$ are the average foil span and chord, respectively, Q is the dynamic pressure, given by (3.18) and V is the boat speed [6][5].

To finalize these matrices we need to replace the variables with their real values. For that we use the prototype values described below.

3.2.1 Prototype Inertia and Geometry

Through various measurements and calculations the boat's properties were determined and are listed here:

Inertia for base configuration

- Mass: 1350 kg
- I_{yy}: 1547.8 kg.m^2

Boat geometry estimates

- L_{boat}: 5 m - Boat overall length
- B: 2 m - Boat beam
- h_{boat}: 2 m - Boat overall height

Inertia extrapolation for heavier configuration

- Mass, m: 1500 kg
- I_{xx}: 1080 kg.m^2
- I_{yy}: 1711 kg.m^2

- I_{zz}: 1500 kg.m^2

Foil geometry estimates from drawings

- x_{HC}; $W_{Fwd} = x_{WF}$: 2.213 m
- z_{HC}; $W_{Fwd} = z_{WF}$: 1.273 m
- x_{HC}; $W_{aft} = x_{WA}$: -1.153 m
- z_{HC}; $W_{aft} = z_{WA}$: 1.293 m
- $y_{FAft} = y_{FA}$: 0.5 m

Foil geometry estimates

- x_{HC}; $W_{Fwd} = x_{WF}$: 2.100 m
- x_{HC}; $W_{Aft} = x_{WA}$: -1.153 m
- z_T : 1.6 m

With that the final open loop matrices defining the boat global dynamics are defined as [6]:

$$A_{global} = \begin{bmatrix} -0.3375 & -0.7689 & -1.9232 & -0.0600 & -9.1054 \\ -2.9227 & -12.09715 & -11.1535 & -5.35857 & -74.5785 \\ -0.4310 & -0.8449 & -32.07000 & -0.8204 & -6.69750 \\ 0 & 1 & 0 & 0 & 0 \\ 0 & 0 & 1 & 0 & 0 \end{bmatrix} \tag{3.31}$$

$$B_{global} = \begin{bmatrix} 0.4793 & -3.8256 \\ -7.34759 & -43.65366 \\ 41.44857 & -44.11284 \\ 0 & 0 \\ 0 & 0 \end{bmatrix} \tag{3.32}$$

Further in section 4.2.3, the closed-loop matrices are computed.

3.2.2 Control Surfaces

These calculations were done for the boat dynamics, so the actuator matrices are still missing. Considering that the actuators are all the same, we can just determine the matrices for one of them. For the 2 states of the actuator, angular position and angular velocity, with an angular rate settling time of 0.2 s and lack of oscillatory motion we have [44]:

$$A_{servo} = \begin{bmatrix} -30 & -225 \\ 1 & 0 \end{bmatrix} \tag{3.33}$$

$$B_{servo} = \begin{bmatrix} 225 \\ 0 \end{bmatrix} \tag{3.34}$$

System Identification

4.1 Introduction

To control a system it is important to have an idea of how it behaves and which are its main characteristics. In a mechanical system we look for its dynamics, how the different masses react to forces and displacements, how it stretches and shrinks, how the energy is dissipated and how it is conserved and converted from kinetic to potential. There are different ways of determining these sets of equations that represent the system described as a model.

Firstly, it is important to have an initial model that represents the system as precisely as it is possible. We can do this through the known laws of physics and by developing force diagrams in Newtonian mechanics [16] or through the equations of energy in the Lagrangian mechanics [8]. The model for the problem in question is based on a theoretical approach where the system is represented as precisely as possible with the known laws that can be applied.

The main problem is that this method relies in a lot of approximations and simplifications that may not apply in the real world. A system will never be theoretically perfect and even if sometimes we can rely on that it is not always the case.

In a complex system like the one being analyzed for a hydrofoil, in this report, the first approach may not be enough. A manual tuning of the controllers may be needed when confronted with real time experiments. With an experienced operator this tuning can be done in the eyes of experience. This also comes with the problem that a tuning for one set of given conditions may not be the most performing for another situation. More specifically in the case of the hydrofoils a different type of environment conditions may impact the system in different ways and cause its instability.

To solve the problem mentioned, a good solution would be the gathering of as much data as possible that includes the biggest variety of possible conditions that the system will encounter. This way we will get information that will minimize the error due to manual tuning and real values that represent the system beyond the theoretical evaluation.

After the data gathering, there needs to be an implementation of identification methods, that through inputs and outputs, can fit a model as precisely as possible. Some of the methods need to be tested for the various conditions and data and compared, through performance metrics, to analyze which ones fit better in the given system.

This last method is also not perfect. To have this measurements as close as

reality as we can get, high quality sensors, capable of measuring all the necessary states and variables, are needed and can end up being expensive. Also the methods used for system identification can have errors and the more complex the system gets, with more inputs and outputs and more intricate variables inner-relations, the more difficult is going to be to define a precise model. However, this method can provide interesting and eye opening results [53].

The identified model in Figure 4.1 consists of two components: a mathematical description of the cause-effect relationships, usually known as the deterministic model and a statistical-plus-mathematical description of the uncertainties, known as the stochastic model.

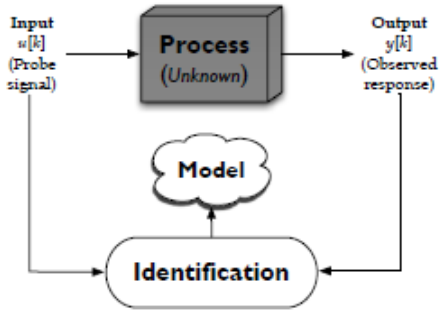

Figure 4.1: Identification using input-output model fitting [53]

The first one is related to the definition of the laws and dynamics that define the system. The second to the presence of noise and errors in the observations. For more introductory and advanced theory the following books are of great use and were an important aid for the development of this project [53][25][13][23][28].

For this project, the first part of the identification process (theoretical determination of the model dynamics), was already done, so here the input-output analysis, through generated theoretical data, is going to be done and various approaches to identify the system are going to be implemented as a first understanding of the identification method. A second analysis was done through simulated data generated in the FaRo software simulator. The end goal would be to apply the identification in real data and compare the results with various metrics, however this was not possible since there were delays with the vessel in question that prohibited the gathering of real test data in the current configuration. Furthermore, the final objective is to have a structure ready to be implemented in real data. Some analysis were still done with previously logged real data to test different hypothesis, regarding data treatment and processing, but the quality was insufficient for complete identification, due to low sampling rates and inappropriate excitations.

4.2 Theoretical Application

Since the system is complex, as well as the methods that are going to be applied, it was more practical to first test the existent functions, for the system identification, in data generated using the first theoretical matrices developed before. This way, we can get a sense of the effectiveness of the methods chosen and use this as the

ground truth data. Also, it is easier to find a pattern in data free of noise and which we know what the result should be.

For that we simplified the system into different dynamics:

- Vertical Dynamics
- Rotational dynamics in relation to y (pitch)
- Vertical Dynamics + Speed
- Full coupled boat actuator dynamics

This way we can analyze the different dynamics of the system separately, being this a good way of knowing it better and understand how the variables react to each other. If everything is shown together, variables can override others and omit important information. Then, when everything is prepared we can start identifying the empirical data.

4.2.1 Generating Data

Firstly, we need to generate our data by creating an input to our state-space equations. With that, get an output to work with. This was done by creating a GBN (Generalized binary noise) [54] sequence, which is a group of step functions, ranging from user-defined minimum and maximum values, number of points, minimum number of points between value change, sample time and probability of change. These system excitations were chosen, since we want to have results regarding as many frequencies as possible. Step functions can be approximated as a sum of an infinite number of sinusoidals, of different frequencies and amplitudes. So, with these inputs we can get valid results that cover all the dynamics required with a simple function. After simulating an output through the state-space equations (2.5), we can call the identification methods on these data sets.

For the practical implementation, the input design requires more attention, since the testing times, budgets and actuators constraints are finite. Also, in real implementation the dynamics can be harder to be excited properly. Later in Section 4.5.5, the design of the inputs for real data is going to be described.

Inputs were simulated for different sampling frequencies such as 20 Hz, 100 Hz and 1000 Hz. 20 Hz due to the fact that the initial data provided had a sampling time of 0.05s (20 Hz), 100 Hz since it is the maximum it can be achieved for the future data to work with and 1000 Hz to evaluate the effect of much higher sampling rates on the identification precision. These inputs were related to the Forward Flap and Aft Flaps average command and were given in rad/s, even if in the graphs they are plotted as deg/s for the reader to interpret the results easier. They can be seen in Figure 4.2.

4.2.2 Identification Methods

System identification methods can be divided into two main categories: Prediction Error Methods (PEMs) and Subspace Identification Methods (SIMs). This report is going to be focused in the SIMs, since they were developed for state space models. PEMs are oriented to identify input-output transfer function models through the

search of system parameters that minimize the errors between the given data and the estimated. The latter methods, are considered to be more precise, however, their computation depends on the solution of nonlinear optimization problems and, for large MIMO systems, that are more complex, they can be unreliable. This is then followed by Singular Value Decomposition (SVD) steps. State space models have a simpler parametrization by performing linear projections of data matrices. Subspace identification methods estimate linear time invariant space models from input-output data [28][42].

After an extensive research, for Python [58] compatible libraries, capable of performing the computations required, it was concluded that the only one available with the proper methods was SIPPY (System Identification Package for Python) [4]. Some methods of this package are also available for Matlab [30] but, in the end, Python was selected due to its easiness for treating data and faster computational speeds. Besides simulation tools and input generation the package also includes PEMs and SIMs. For the purpose of this work 3 of the methods defined in the package are going to be used: MOESP [19][18] PARSIM-K [42], N4SID [19][18][56].

N4SID and MOESP are two of the main algorithms utilised for subspace identification. They are based on QR (Q: orthogonal matrix, R: upper triangle matrix) decomposition, SVD, matrices projection and the angles of subspaces that are robust linear algebra numerical tools for multivariable systems [57].

The PARSIM-K method is an identification algorithm with parsimonious (using the minimum number of parameters as possible) model parametrization. Usually there is a trade-off between good fit of identification and number of parameters. A parsimonious model can represent a system better if well performed, since is more reliable for the prediction with other data sets, having a direct relation with the real parameters. High parameter models can have good short term fitness but not work as well for the prediction with other data sets, having an indirect relation with the real parameters [42].

In this report the depths of the linear algebra, needed for the description of these methods, is not going to be reviewed since if out of its scope. These methods will be tested for different data sets and compared.

One of the problems for identifying systems is the determination of the model order. There are several methods to calculate an estimate for the most probable order, like the Akaike information criterion [1]. For our model, since there was an extensive theoretically model development we can assume the order of the model to be the number of states defined, due to the fact that they are the minimal number of variables that we need to fully describe the current situation of our system.

After simulating the data we will try several sub-space identification methods and compare their results both for initial data and for validation data to verify the correctness of the system's parameters determination.

These methods are going to be applied through a function from the SIPPY package. This function, system_identification(), takes as parameters the inputs and outputs, the method wanted (in this case MOESP, N4SID and PARSIM-K), order of the system, time sample, number of iteration, requirement of the D matrix to be zero or not and past and future horizons.

The use of this function presents some obstacles that need to be solved through different manipulations. These are:

- Some A and B matrices calculations were giving values that were erroneous,

because it is known that there exists 1 to 1 and null relations between some states and other states derivatives. These are defined with rows with zeros and ones. Since that is a predetermined constraint, it is going to be imposed manually and compared to a not constrained version.

- The system_identification() function, does not allow the user to define C as an identity matrix as a restriction. And in the case of this study this is important, since the states defined are the ones that are going to be analyzed by the user and that are needed for the boat stability and performance analysis. This can be changed with ease with a change of basis operation.
- The theoretical matrices were derived for a continuous-time system, whereas the ones calculated from the simulation results were determine for a discrete-time system.

All of these obstacles can be solved and its solution is going to be shown in the next section.

4.2.3 Matrix Manipulation

Now that the different steps required for the identification of the system are defined, we can start by applying this logic.

To begin the application some theory needs to be discussed for the comprehension of further developments. The first step is to analyze the initial order reduction required to establish the pre-determined, well known, zeros and ones that define null or equivalent relation between variables.

Considering the following matrices A and B:

$$A = \begin{bmatrix} x_1 & x_2 \\ 1 & 0 \end{bmatrix} \tag{4.1}$$

$$B = \begin{bmatrix} x_3 & x_4 \\ 0 & 0 \end{bmatrix} \tag{4.2}$$

where the values x are the constants that need to be determined through system identification. The last rows are known so it is possible to impose those values by some manipulation. By removing the last column of matrix A, and considering these system as having only 1 state (A is 1×1) we can transfer this column to be the first column of B (B is now 1×3) and define an extra input, as being the state we are transferring to B. The matrices would now be:

$$A = \begin{bmatrix} x_1 \end{bmatrix} \tag{4.3}$$

$$B = \begin{bmatrix} x_2 & x_3 & x_4 \end{bmatrix} \tag{4.4}$$

$$\tag{4.5}$$

Remaining the 4 unknown constants that are going to be determined. Since the state space equations defined in (2.5), represent a linear, time-invariant combination of parameters, the results and the transformation is valid. At the end of all calculations, the first value of B can be re-transferred to A to the same position as it was and the final rows of both matrices are implemented as being [1,0] for A and [0,0] for B. This method is independent of the size of the matrices whilst there exists a 1 to 1 or null relation between the derivative of the variable being transferred and a state that remains in the A matrix. Thus, this can be done with the height and pitch columns, since there is always going to be their derivatives as a state.

The next step will be done after the identification process, along with the re-organization of matrices A and B, to transform the matrices from discrete-time to continuous. This is because the theoretical matrices are determined for continuous time and in order to compare the identified ones (from discrete signals) with the theoretical ones, a conversion is needed. One of the simpler methods to compute this approximation is the Euler's method [17]. By considering the first derivative as $t = kT$ with k being the time step defined and T the time sample. With that being said we can define:

$$\dot{x}(t) = \frac{dx(t)}{dt} \approx \frac{1}{T}(x((k+1)T) - x(kT)) \tag{4.6}$$

merging (4.6) and (2.5) we get

$$\frac{1}{T}(x((k+1)T) - x(kT)) \approx Ax(kT) + Bf(kT) \tag{4.7}$$

$$x((k+1)T) \approx (I + TA)x(kT) + TBf(kT) \tag{4.8}$$

$$x[k+1] \approx (I + TA)x[k] + TBf[k] \tag{4.9}$$

where

$$A_d = I + TA, \quad B_d = TB \tag{4.10}$$

and d is a subscript for 'discrete'. With these simple calculations we can convert the discrete time to the continuous time and the problem is solved.

Finally, the transformation of the C matrix to the identity matrix can be done with a change of basis of the equations. There are infinite representations for a system, so the one given by an identification process can be different of the one used for the simulation. Through some manipulation, it is possible to approximate both solutions. The first step was already done, now the focus is on getting C to be an identity matrix. Considering z the identified values for the states and A_Z, B_Z and C_Z, the identified matrices we get:

$$\dot{z} = A_Z z + B_Z u \tag{4.11}$$

$$x = C_Z z \tag{4.12}$$

so,

$$z = C_Z^{-1} x \tag{4.13}$$
$$C_Z^{-1} \dot{x} = A_Z C_Z^{-1} x + B_Z u \tag{4.14}$$
$$\dot{x} = C_Z A_Z C_Z^{-1} x + C_Z B_Z u \tag{4.15}$$

In the end we get:

$$A = C_Z A_Z C_Z^{-1}, \quad B = C_Z B_Z \tag{4.16}$$

Important to notice that C needs to be invertible, and that the order of the system needs to correspond to the number of outputs defined [10].

Now that the theory has been outlined, it can be applied to the generated data and to the different dynamics of the boat, from simpler to more complex.

4.2.4 Closed-Loop Matrix

From the work in [6] the theoretical matrices for the open-loop system were determined in section 3.2. For the theoretical generation of data, the matrices should be representing the closed-loop to illustrate properly the usage of real data, since the system is highly unstable, while in open-loop, and the gathering of data can involve unnecessary risks.

In equation (2.14) it was shown that the $A_{cl} = A_{global} - BK$. Considering the matrix K, shown in 4.17, pre-determined through manual tuning in the SB4 tests, A_{cl} can be calculated.

$$K = \begin{bmatrix} 0.10470 & 0.08376 \\ -0.10091 & -0.08073 \\ 0.70000 & -0.32550 \\ -0.83538 & -0.66830 \\ 3.50000 & -1.62750 \end{bmatrix}^{\intercal} \tag{4.17}$$

A_{cl} becomes

$$A_{cl} = \begin{bmatrix} -0.06729 & -1.02933 & -3.503944 & -2.21627 & -17.00908 \\ 1.50303 & -16.36277 & -20.21948 & -40.67052 & -119.90820 \\ -1.07577 & -0.22351 & -75.44272 & 4.32406 & -223.56116 \\ 0 & 1 & 0 & 0 & 0 \\ 0 & 0 & 1 & 0 & 0 \end{bmatrix} \tag{4.18}$$

4.3 Identification Evaluation Metrics

Different metrics were gathered in order evaluate the quality of a system's identification. They will be displayed accordingly.

4.3.1 Best Fit Criterion

Computing the best fit criterion, based on the explained variance between two data sets, demonstrated by equation (4.19), we get a measure of the 'fitness' of the identified system [45].

$$Fit[\%] = (1 - \frac{\sqrt{\sum_{k=1}^{N}(y(k) - \hat{y}(k))^2}}{\sqrt{\sum_{k=1}^{N}(y(k) - \bar{y})^2}}) \times 100 \tag{4.19}$$

where $y(k)$ represents the real values, $\hat{y}$ the predicted values and $\bar{y}$ the real values average. Important to note that the effect of the variance for an almost constant signal, will be low, decreasing the value of fitness. So if a system is not excited properly the identification of an almost constant state is not as reliable, since there can be a marginal error and sill have low fitness. This will be explained in detail in Section 4.6.2.

4.3.2 Relative Error (RE) and Root Mean Square Error (RMSE)

The RE, (4.20) and the RMSE, (4.21) can be important to serve as a confirmation of the fitness values. For fitness values averaging 90-99%, usually, the best fit criterion portraits properly the quality of the system identification. However for lower fitness values the result can be less accurate.

Analyzing an identified state that has a low value of fitness regarding the gathered data, lets say below 50% , it can be noticed that sometimes the curves do not match but they are separated constantly by a small neglectable margin.However, this small margin can be invisible in a fitness value if the signal variance is even lower. Small errors between two signals but with even smaller variances correspond to smaller values of fitness, as it can be deducted from equation (4.19).

$$RE = \frac{y_i - \hat{y}_i}{max(y_i)} \tag{4.20}$$

$$RMSE = \sqrt{\frac{1}{N}\sum_{i=1}^{N}(y_i - \hat{y}_i)^2} \tag{4.21}$$

The application of identification metrics and its further explanation will be showed, with more detail, in Section 4.6.2. This is needed specially for lower fitness values and in real data sets this happens.

4.4 Identification Methods Evaluation

Vertical Dynamics

As we are interested in the vertical dynamics, an intersection of the 2nd and 4th rows and columns is going to be used. These are the values corresponding to the vertical displacement, rate, and its inner relation. They represent the vertical dynamics of the system, as it can be seen from (4.22) to (4.25):

$$A_{vert} = \begin{bmatrix} -16.36277 & -40.67052 \\ 1 & 0 \end{bmatrix} \tag{4.22}$$

$$B_{vert} = \begin{bmatrix} -7.34759 & -43.65366 \\ 0 & 0 \end{bmatrix} \tag{4.23}$$

$$C_{vert} = \begin{bmatrix} 1 & 0 \\ 0 & 1 \end{bmatrix} \tag{4.24}$$

$$D_{vert} = \begin{bmatrix} 0 & 0 \\ 0 & 0 \end{bmatrix} \tag{4.25}$$

By using the forced_response() function from the control package it was possible to simulate the height and height rate states from the system dynamics matrices and inputs defined, in this case the excitation was between -1 and 1 degrees for the forward flap and average aft flap, with a minimum of 20 time steps per input variation and this variation, with a 50% probability of occurring. In Figure 4.2 an example of data generation for a frequency of 100 Hz is shown.

Now that the inputs and outputs are determined, they are ready to be introduced in the system identification functions.

The identification is going to be implemented in two different ways:

- With no previous matrix manipulation besides changing basis for C to be an identity matrix and convert from discrete to continuous-time. No constraints for ones and zeros.
- With the whole manipulation discussed before.

This way we can confirm the effectiveness of the method and in which way, the system fits better the data. Furthermore we are going to name the non manipulated results as "original" and the manipulated results as "1 state". The practical difference is going to be in three parameters given to the identification function - the inputs, the outputs and the system order. For the original data the order is going to be 2, due to the 2 states present in matrix A and for the "1 state" the order is going to be only 1, with the inputs being now defined as $u_{1state} = [\delta Z \ \delta_{FF} \ \delta_{FAAvg}]$. The inputs for the original results remain the same $u_{original} = [\delta_{FF} \ \delta_{FAAvg}]$. The outputs vector will have the same dimension as the states vector for each set of data, 1 for the 1 state case and 2 for the original.

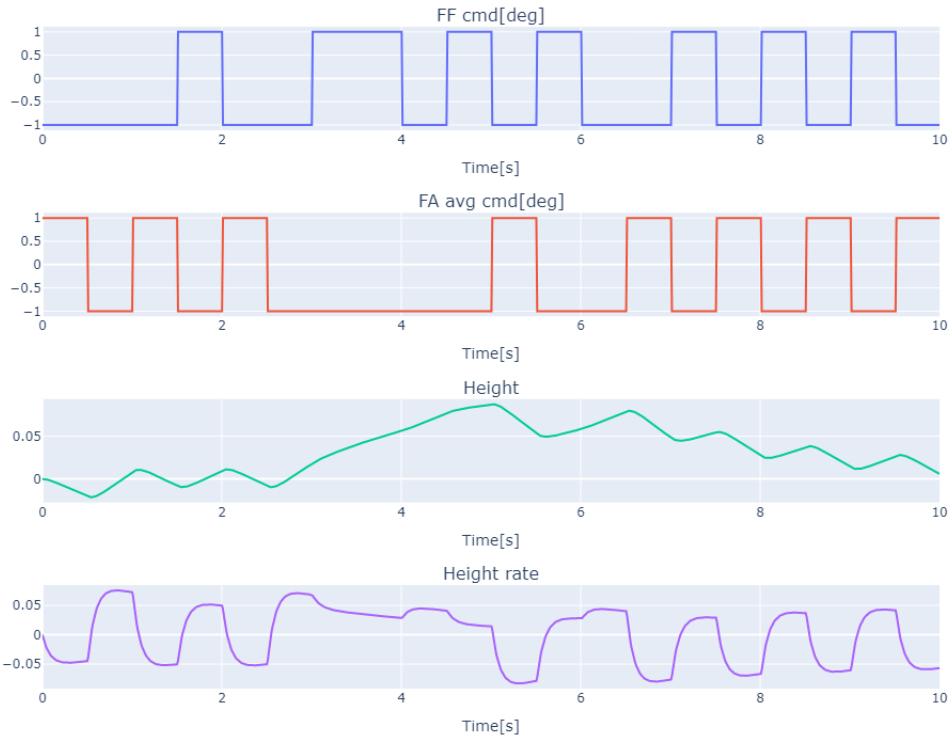

Figure 4.2: Vertical dynamics response and inpunts

After the identification is done, the two final steps are applied, converting the matrices to continuous time and changing the basis to have an identity matrix for C.

Finally, to get our last approximation to the matrices calculated, for the "1state" values, we need to force the last rows of the matrices A and B to be [1 0] and [0 0] respectively and return the state moved to B, to A and have the final dimensions as they were originally and with the correct structure.

Now that the identification process is complete, it is time to compare the fitness of each system in relation to the original data. Also validation with a different set of inputs is done to confirm if the identified values add up for a different excitation.

In Tables 4.1 and 4.2 it is possible to see the different results for the height and height rate fitness, respectively, for the various identification methods and for the original, non manipulated, matrices (Org) and the manipulated matrices (1State). Also, the "1st" refers to an initial matrix identification for a given data set and the "test" refers to the validation data set, implemented to the "1st" identified matrices, in order to test the generalization of the identified matrices.

A helpful measure to take into account is the comparison between the fitness of the original identification (without the post-process manipulation) and the fitness of the 1 state matrices. In general, the original identification provides better results across the 3 methods and the only method providing good identification for the 1 state matrices is "PARSIM-K". When the result is given by "——", it is because the

Height Fitness [%] - 20 samples average						
Method	Org 20 Hz	1state 20 Hz	Org 100 Hz	1state 100 Hz	Org 1 KHz	1state 1 KHz
1st PARSIM-K	91.8243	93.3422	98.3077	98.9192	99.7908	99.8541
test PARSIM-K	91.4611	92.676	98.0643	98.8078	99.7673	99.8473
1st N4SID	92.9742	—-	98.4251	53.9169	99.8486	93.8723
test N4SID	92.0013	—-	98.1629	61.4472	99.8254	92.9929
1st MOESP	92.3605	—-	98.3432	57.5372	99.8398	91.795
test MOESP	91.3792	—-	98.1729	59.1116	99.8205	91.7244

Table 4.1: Vertical dynamics height fitness results

Height Rate Fitness [%] - 20 samples average						
Method	Org 20 Hz	1state 20 Hz	Org 100 Hz	1state 100 Hz	Org 1 KHz	1state 1 KHz
1st PARSIM-K	90.3399	93.5095	98.5393	98.8767	99.8291	99.8475
test PARSIM-K	90.167	93.4424	98.5511	98.8915	99.8326	99.8513
1st N4SID	86.5053	—-	97.6043	85.0308	99.7709	98.3887
test N4SID	85.5778	—-	97.5636	86.3447	99.7557	98.4364
1st MOESP	86.07	—-	97.6487	85.6036	99.7686	97.754
test MOESP	85.8022	—-	97.4776	86.7076	99.7617	97.9048

Table 4.2: Vertical dynamics height rate fitness results

values were unstable and the fitness of those methods for a given frequency were not positive.

A process similar to this, applied to the vertical dynamics, was applied to other dynamics and is described below.

Pitch Dynamics

Proceeding to the Pitch dynamics, the first step is going to be to simulate data through the theoretical matrices calculated before. The A and B matrices used are represented in equations (4.26) and (4.27) where the C and D matrices are the same. These values were taken from the intersection of the 3rd and 5th rows/columns of the matrix A_{cl}, representing the pitch rate and the pitch variation, respectively.

$$A_{pitch} = \begin{bmatrix} 75.44272 & 223.56116 \\ 1 & 0 \end{bmatrix} \tag{4.26}$$

$$B_{pitch} = \begin{bmatrix} 41.44857 & -44.11284 \\ 0 & 0 \end{bmatrix} \tag{4.27}$$

The same identification package was used throughout the different dynamics, so no more explanation of the current process is needed. In this case, the state that is moved to the inputs is the pitch variation. Tables 4.3 and 4.4 show the results for the pitch and pitch rate fitness, respectively.

Again, as it happened with the Vertical dynamics, results remain unstable for the 1state at 20 Hz for the N4SID and MOESP methods. However, the trend continues from the 100 Hz mark and the results get better. Curiously for the original 100

Pitch Fitness [%] - 20 samples average						
Method	Org 20 Hz	1state 20 Hz	Org 100 Hz	1state 100 Hz	Org 1 KHz	1state 1 KHz
1st PARSIM-K	91.2566	87.2125	—	94.5615	99.5263	99.5261
test PARSIM-K	89.2564	80.8166	—	93.8823	99.2931	99.2826
1st N4SID	94.2426	—	98.6298	32.7532	99.8514	80.5879
test N4SID	93.2336	—	98.7085	24.3687	99.8331	80.8795
1st MOESP	94.2296	—	98.6003	36.4125	99.849	71.3498
test MOESP	92.7255	—	98.5648	12.1585	99.8235	71.5361

Table 4.3: Pitch dynamics pitch fitness results

Pitch Rate Fitness [%] - 20 samples average						
Method	Org 20 Hz	1state 20 Hz	Org 100 Hz	1state 100 Hz	Org 1 KHz	1state 1 KHz
1st PARSIM-K	81.3068	89.2371	—	96.1184	99.6171	99.6211
test PARSIM-K	79.9494	88.607	—	96.0151	99.6024	99.6062
1st N4SID	80.5766	—	96.4928	79.7765	99.6574	96.6194
test N4SID	79.1868	—	96.0039	79.4202	99.6404	96.7883
1st MOESP	80.3182	—	96.4627	79.4118	99.6556	95.4774
test MOESP	78.8648	—	95.9742	80.2347	99.6294	95.2301

Table 4.4: Pitch dynamics pitch rate fitness results

Hz data the PARSIM-K method fails to identify the system. The reason remains unsolved. 1 KHz data reinforces the statement that as sampling rate increases so does the identification quality.

Vertical + Longitudinal Speed Dynamics

Following the same procedure as before, equations (4.28) and (4.29) represent the theoretical matrices regarding the vertical dynamics plus the longitudinal speed. Once again for the 1 state fitness calculation, the height state is transferred as an input to the identification. Tables 4.5, 4.6 and 4.7 show the results for the speed, height rate and height, respectively.

$$A_{spd+vert} = \begin{bmatrix} -0.06729 & -1.02933 & -2.21627 \\ -1.50303 & -16.36277 & -40.67052 \\ 0 & 1 & 0 \end{bmatrix} \tag{4.28}$$

$$B_{spd+vert} = \begin{bmatrix} 0.4793 & -3.8256 \\ -7.34759 & -43.65366 \\ 0 & 0 \end{bmatrix} \tag{4.29}$$

Results for the vertical + longitudinal speed dynamics are similar to the ones of the vertical dynamics. These only differ from the previous pitch results in the original 100 Hz data.

Speed Fitness [%] - 20 samples average						
Method	Org 20 Hz	1state 20 Hz	Org 100 Hz	1state 100 Hz	Org 1 KHz	1state 1 KHz
1st PARSIM-K	92.8907	89.2697	98.7372	95.3996	99.7793	96.2485
test PARSIM-K	85.7086	73.3201	97.9489	72.7827	99.6509	94.5056
1st N4SID	96.7217	—-	99.3386	82.5221	99.9193	96.9025
test N4SID	96.2118	—-	99.2452	76.3019	99.9009	96.0705
1st MOESP	96.6979	—-	99.3036	77.58	99.9284	91.0126
test MOESP	95.992	—-	99.1725	71.8158	99.9153	89.1672

Table 4.5: Vertical + Longitudinal speed dynamics - speed fitness results

Height Rate Fitness [%] - 20 samples average						
Method	Org 20 Hz	1state 20 Hz	Org 100 Hz	1state 100 Hz	Org 1 KHz	1state 1 KHz
1st PARSIM-K	89.8979	91.7422	98.4961	95.5805	99.8242	96.9449
test PARSIM-K	89.2668	90.9955	98.495	93.7497	99.8279	97.0562
1st N4SID	86.4279	—-	97.7041	90.2651	99.7798	98.8283
test N4SID	84.882	—-	97.4666	90.3591	99.7468	98.9015
1st MOESP	86.1675	—-	97.6505	88.985	99.7739	95.715
test MOESP	85.5754	—-	97.4748	89.9942	99.7639	96.1701

Table 4.6: Vertical + Longitudinal speed dynamics - height rate fitness results

Height Fitness [%] - 20 samples average						
Method	Org 20 Hz	1state 20 Hz	Org 100 Hz	1state 100 Hz	Org 1 KHz	1state 1 KHz
1st PARSIM-K	91.1526	90.8987	98.3623	94.1561	99.7879	96.721
test PARSIM-K	89.3672	85.7501	98.0567	78.5411	99.7826	96.0042
1st N4SID	92.3217	—-	98.4488	78.055	99.8438	97.2462
test N4SID	91.7061	—-	98.3328	73.9326	99.8316	96.1841
1st MOESP	92.926	—-	98.5102	73.2483	99.8509	89.6941
test MOESP	92.059	—-	98.1935	67.8186	99.8171	88.3094

Table 4.7: Vertical + Longitudinal speed dynamics - height fitness results

Global Dynamics

Finally the identification methods were applied for the global dynamics, after the interpretation of the separated dynamics. In this case the pitch and height variables were given as an input to the identification functions and reorder later into the states as originally shown. A_{cl}, (4.18), and B_{global}, (3.32), matrices were used to generate the data. Tables 4.8, 4.9, 4.10, 4.11 and 4.12 show the results for the speed, height rate, pitch rate, height and pitch fitness, respectively.

Conclusion

From analyzing the tables for the fitness results, it is clear that with increasing sampling rate the results tend to be better. Looking, for example, at N4SID for the original matrices, fitness values can increase from 82% to 99%, from 20 Hz to 100 Hz. This is because the data is more insightful, describing the system better and not disregarding important dynamics. Even though, for real systems, a sampling rate that is too high can incorporate unwanted noise and can be unfeasible with the equipment provided, a compromise should be made between precision and noise.

More importantly identification with 100 Hz data is clearly possible, since its original identification fitness for the various methods wanders around 85% to 95%. Real and simulation data, to be used, are going to be in that frequency range.

Speed Fitness [%] - 20 samples average						
Method	Org 20 Hz	1state 20 Hz	Org 100 Hz	1state 100 Hz	Org 1 KHz	1state 1 KHz
1st PARSIM-K	89.4233	67.9906	82.9201	81.7193	99.1808	98.6147
test PARSIM-K	75.0103	64.46	84.2676	74.3253	98.579	94.2369
1st N4SID	95.7996	—-	99.2003	63.5164	99.9193	96.9025
test N4SID	95.8415	—-	99.1792	43.5563	99.9135	30.5343
1st MOESP	95.8151	—-	99.1892	19.3015	99.904	—-
test MOESP	95.7425	—-	99.1466	23.8257	99.9173	—-

Table 4.8: Global dynamics - Speed fitness results

Height rate Fitness [%] - 20 samples average						
Method	Org 20 Hz	1state 20 Hz	Org 100 Hz	1state 100 Hz	Org 1 KHz	1state 1 KHz
1st PARSIM-K	87.8127	78.7039	95.7883	84.155	99.6101	98.4892
test PARSIM-K	85.2309	81.5419	93.8167	86.0132	99.1728	98.2459
1st N4SID	89.3213	—-	97.8069	86.1084	99.782	82.8947
test N4SID	85.2858	—-	96.5054	79.6321	99.7552	72.5366
1st MOESP	89.2984	—-	97.8544	40.7907	99.7778	—-
test MOESP	88.6259	—-	96.9583	35.5849	99.7263	—-

Table 4.9: Global dynamics - Height rate fitness results

Pitch rate Fitness [%] - 20 samples average						
Method	Org 20 Hz	1state 20 Hz	Org 100 Hz	1state 100 Hz	Org 1 KHz	1state 1 KHz
1st PARSIM-K	88.8422	95.1417	96.0991	98.2764	99.6059	99.7751
test PARSIM-K	86.7328	94.7427	95.5075	98.2812	99.4254	99.6893
1st N4SID	84.424	—-	96.9516	94.5718	99.6782	94.0754
test N4SID	82.394	—-	94.4327	91.5615	99.6413	88.6867
1st MOESP	85.1962	—-	96.9944	77.1763	99.9284	—-
test MOESP	82.7918	—-	95.5834	67.1727	99.9153	—-

Table 4.10: Global dynamics - Pitch rate fitness results

Height Fitness [%] - 20 samples average						
Method	Org 20 Hz	1state 20 Hz	Org 100 Hz	1state 100 Hz	Org 1 KHz	1state 1 KHz
1st PARSIM-K	88.238	62.5957	89.2772	78.2769	99.3384	98.8839
test PARSIM-K	77.5593	65.5691	86.4472	78.6932	98.652	97.187
1st N4SID	95.663	—-	99.1537	82.0848	99.9138	60.3827
test N4SID	96.1675	—-	99.1326	64.485	99.8996	57.117
1st MOESP	95.1489	—-	99.2123	34.0837	99.9284	—-
test MOESP	95.7067	—-	99.0829	—-	99.9153	—-

Table 4.11: Global dynamics - Height fitness results

Pitch Fitness [%] - 20 samples average						
Method	Org 20 Hz	1state 20 Hz	Org 100 Hz	1state 100 Hz	Org 1 KHz	1state 1 KHz
1st PARSIM-K	88.729	61.4764	90.1151	77.7402	99.3343	99.3857
test PARSIM-K	79.5934	63.7982	85.6479	79.2944	98.69	99.0446
1st N4SID	95.5872	—-	98.9063	84.6557	99.8715	52.0227
test N4SID	95.8108	—-	98.8656	66.1861	99.87	64.3842
1st MOESP	94.5095	—-	98.9485	35.3241	99.9284	—-
test MOESP	94.5095	—-	98.7238	22.6472	99.9153	—-

Table 4.12: Global dynamics - Pitch fitness results

An iterative process should be useful to realize which frequencies of the system's dynamics are of importance to determine the optimum sampling rate. Considera-

tions about this are developed in Section 4.5.5

The 'PARSIM-K' method seems to be the only one consistently compatible with the matrix manipulation data '1 state', thus being of interest when applying to real data after the model order reduction.

'N4SID' and 'MOESP' have a similar approach to the identification process, however, 'N4SID' provides slightly better results for almost every section of the testing, specially when more states are in play. N4SID should be used as the primary method for identification and MOESP as a backup to confirm the previous statements.

4.5 Real Data Application

In this section, a process for identifying real data systems is discussed. This includes ideas about data generation and treatment, since the overall process relies on the same methodologies applied in theoretical data, besides the part of irregularities present in data due to several random phenomena. Figure 4.3 summarizes the process defined and is useful for the reader to follow along.

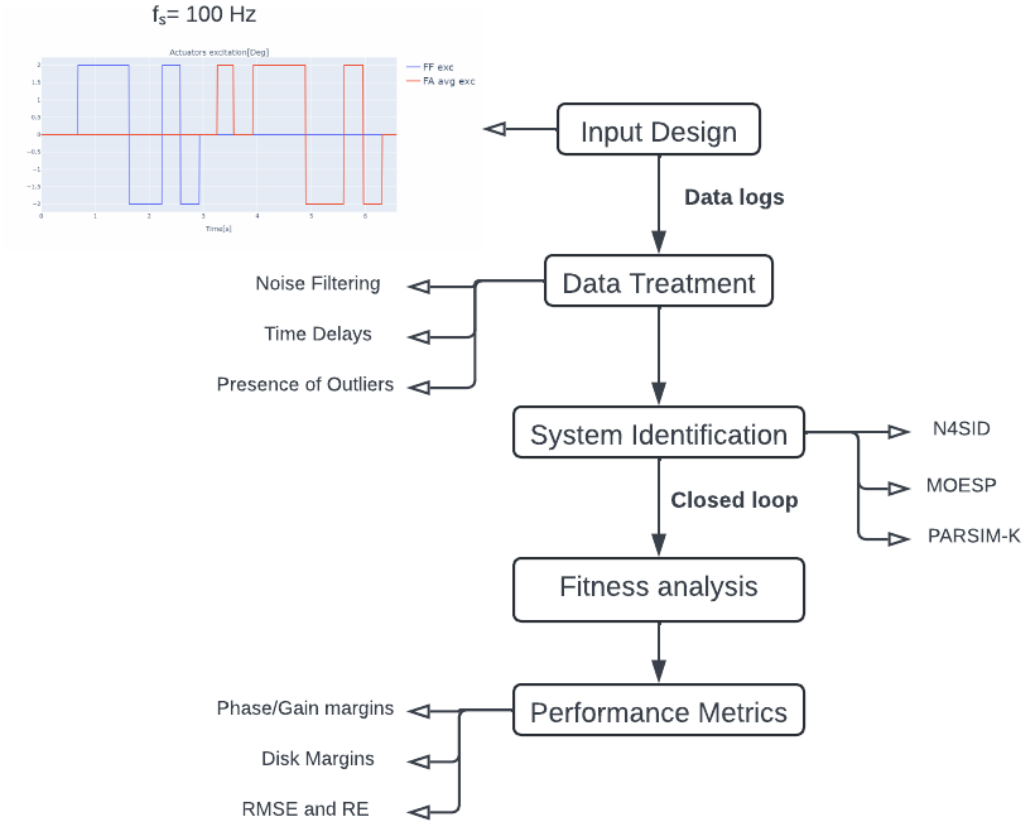

Figure 4.3: Final process diagram

4.5.1 Gain Matrix Speed Linearization

As it was discussed previously, the dynamics of the boat will change with the variation of its velocity, this due to the lift and drag forces being proportional to the square of the speed (section 3).

Instead of considering all the nonlinearities and how they manipulate the system's dynamics a straightforward quadratic compensation is used to relate the boat's controller gain changes with the average speed during a certain time interval (V_{avg}) and a reference speed (V_{ref}). This equation is given by (4.30).

$$K_{lin} = \frac{V_{ref}^2}{V_{avg}^2} \tag{4.30}$$

K_{lin} is the constant calculated that will multiply the K original matrix to produce a final linearized speed matrix in relation to a boat reference speed and K matrix.

4.5.2 Noise Analysis

When utilising real data, instead of computer generated data, some problems were identified regarding the quality of it. These are related to delays, excess of noise from the measurements, presence of outliers, aliasing of the signals, etc. In this section these obstacles and their determination and solutions are addressed.

One of the major key points of system identification is data quality. If the data is not precise, then the identification is going to give misleading responses, since it is not representing reality but a distorted version of it. There are various aspects that contribute to the quality of the data from the sampling rate to the noise present in it [53].

For multiscale systems, with phenomena that occur on diverse time scales rather than a universal one, sample rate selection might be an issue. A compromise must be found that optimally obtains data from relevant dynamics, while avoiding noise excess. In relation to noise, it is true that as the sample rate increases, the precision of the data acquired increases, because the data will be more complete, filling in the gaps that lower sampling rates would leave empty. However, with higher sampling rates, undesirable phenomena are gathered. These unwanted data can be denominated as noise and is dependent on external variations that are uncorrelated with the system [53].

Even if measurements to reduce noise are taken, such as vibration damper implementation, there is still going to be noise present. However, it is possible to remove frequencies of the signal that may be interfering with the data quality using frequency analysis. The data will be subjected to post-processing filtering in order to remove as much noise as feasible.

For this system data was gathered in the testing of Seabubbles SB4 boat with a sampling rate of 50 Hz. For the excitation of all the system's important frequencies, step excitations were induced in the different control surfaces of the boat.

The noise was removed for all variables that will be used in the system identification procedure, which are those defined in the equations (3.3) and (3.1). To get a sense of the essential frequency components from each variable, the first step is to translate from the time domain to the frequency domain. Figure 4.4 shows the height state, frequency components, as an example. Through the graphical representation,

it is possible to compute which frequencies have predominant influence and where is it possible to define a cutoff frequency. After that, a Butterworth fourth-order zero-lag low-pass filter is applied to remove the higher frequencies from the signal with no lag (by passing the filter twice in opposite directions) [52]. Different low pass filters like the Chebyshev or the Bessel filter could have been used, however the Butterworth filter was applied due to its linear gain decrease and easiness of determining the frequencies that are being passed. In this study, a method was utilized to translate to the frequency domain, which is discussed in [25] and described in Appendix A. In [61] a method was developed to find an optimum cutoff taking into consideration not only the sampling rate but also a mean residual error. This method consists in 4 steps:

- Determine a cutoff frequency taking into account the sampling rate using (4.31)
- Filter the data by the frequency determined
- Compute the mean residual error between the filtered and non filtered data
- Calculate the final cutoff frequency with equation (4.33)

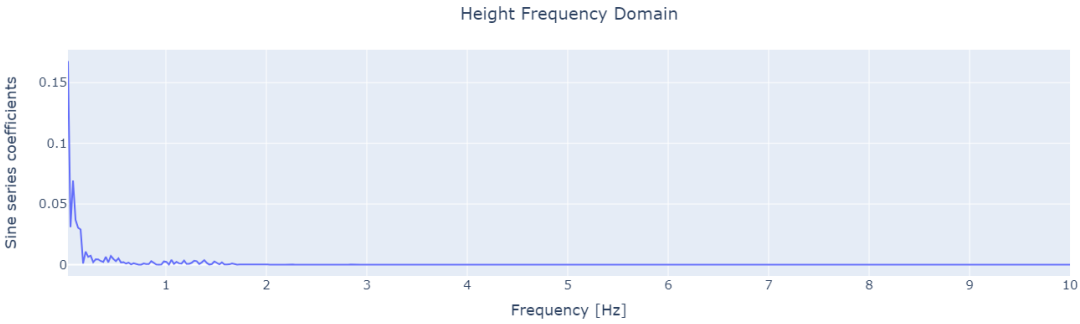

Figure 4.4: Height in the frequency domain

In [61] a correlation was found between the optimum cutoff frequency and the sampling frequency through several regressions for different data with different noises and time samples. With that equation (4.31) was found.

$$f_c = 0.071 f_s - 0.00003 f_s^2 \tag{4.31}$$

where f_c is the first cutoff frequency solely influenced by f_s (sampling frequency). After filtering the original data the final step can be done by firstly computing the mean residual error (4.32) followed by the final cutoff frequency with equation 4.33

$$\epsilon = \sqrt{\frac{\sum_{n=0}^{N}(x_n - x_n')}{\sum_{n=0}^{N}(x_n - \bar{x})^2} * 100\%} \tag{4.32}$$

$$f_{c2} = 0.06 f_s - 0.000022 f_s^2 + 5.95 \frac{1}{\epsilon} \tag{4.33}$$

$\bar{x}$ is the mean of x_n, the original data, and $x_n^{'}$ is the filtered data set for f_c.

This method gives an estimation of the cutoff frequency taking into consideration the noise present in a given signal. However, for signals with almost no noise, f_{c2} would be too high (higher than the Nyquist frequency), so in those cases the cutoff frequency should be determined by the user's interpretation given the visual interpretation of the signal in the frequency domain and the cutoff frequency associated with the chosen sampling rate, f_c.

Finally, for different samples the noise can be different, this can be approximated for similar testing conditions but it should be noticed that the cutoff values can change in between data sets due to variation in the testing conditions and unpredictable phenomena.

As an example, different fitness values for identification processes are shown, in pre and post filtered data. In table 4.13, the different calculated values for the cutoff frequencies are shown. SNR (signal to noise ratio), represents the relation between the power of a signal and the noise content in it. In theory, usable results should have a minimum SNR of 3 [25]. Some of the variables in analysis, like the height and pitch rates, are not compatible with this criterion, however, the data used in this section, was for testing only of the filtering processes.

Variable	SNR	f_c [Hz]	f_{c2} [Hz]	Visual [Hz]	Final [Hz]
FF	3.90	3.4750	20.2237	5	5
FA Avg	7.23	3.4750	8.6142	7	7
Speed	127	3.4750	11.2236	2	2
Height Rate	0.0015	3.4750	5.8890	5	6
Pitch Rate	0.0016	3.4750	5.9800	5	6
Height	17.73	3.4750	16.6100	2	2
Pitch	0.7141	3.4750	25.6700	4	4

Table 4.13: Noise filtering values

Looking at table 4.13 besides the frequencies f_c and f_{c2} a cutoff frequency determined visually is displayed alongside the final determined cutoff frequency. To determine the final frequency, different cutoff values were tested, for the same data set, and the filtered data was inputted into the system identification function. The "Final" cutoff frequency values selected were the ones that originated the higher identification fitness.

It can be concluded that for noisy signals, with low SNR, f_{c2} can be a reliable optimum cutoff frequency. The Pitch state, even if it has higher SNR, its noise contents are predominantly on the low frequencies so f_{c2} is exaggerated . In the end, the visual cutoff frequency worked the best. The rest of the variables have high SNR so this means that their noise content is relatively low. After testing the different cutoff frequencies for the rest of the states and inputs (FF, FA Avg, Speed and Height) it was concluded that the visual method ends up being the best since f_{c2} is underwhelming.

Before filtering the fitness results were unstable and extremely negative which was unfeasible. After filtering, the values are given in table 4.14 and are positive and stable, with the exception of speed. A possible explanation about the low values of speed fitness is given in Section 4.6.2.

State	Fitness [%]
Speed	-36
Height Rate	45.53
Pitch Rate	54.45
Height	24.47
Pitch	70.791

Table 4.14: Fitness results after noise filtering

4.5.3 Signal Delays

Besides the noise coming from various phenomena involved in the data gathering process there can also be problems related with the delay of specific signals that occur due to electrical/communication issues and not from the inherent dynamics of a system. This can be seen when utilising a controller that manages different input signals, taking a finite amount of time transforming them to the outputs required.

In the case of this hydrofoil analysis delays can occur in the FCS (foiling control system) and it is possible to evaluate them, through signal cross-correlation, calculating which signal time step translation corresponds to the biggest similarity between them. In order to have a more intuitive result in a form of a coefficient instead of a disproportional number, the correlation coefficient, r, is demonstrated in relation to the square root of a ratio of the auto-correlation of each signal, equation (4.35). Equation (4.34) shows how the cross-correlation, z of two discrete, finite signals, x and y, is computed for a number of points N where k represents the time step of the delay, thus the equivalent delay in seconds being k*Δt.

$$z_{x,y}[k] = \sum_{l=0}^{||x||-1} x_l y^*_{l-k+N-1} \qquad k = 0, 1, ..., ||x|| - 1 \tag{4.34}$$

$$r(k) = \frac{z_{x,y}(k)}{\sqrt{z_{y,y}\left(\frac{||y||}{2}\right) z_{x,x}\left(\frac{||x||}{2}\right)}} \qquad ||x|| = ||y||, k = 0, 1, ...||x|| - 1 \tag{4.35}$$

where .* accounts for the conjugate of the vector and $||x||$ for the length or number of points of the signal vector and it is subtracted by 1 due to the nature of Python indexing starting in 0. Since the signals in question consist in real numbers the conjugate is redundant. These functions were implemented through the Python package "SciPy".

Important to note that the correlation coefficient of a specific time lag can be marginally higher than the 0 lag coefficient, which means, that the time difference between the signals can be neglected. Due to that both the maximum correlation and the 0 lag correlation coefficients were computed and compared along with a visual interpretation of the signals.

As an example of the noise delay analysis being applied, Figure 4.5 shows two signals which are delayed approximately by one time sample interval (0.02 s - 50 Hz) and Figure 4.6 the respective delay and cross-correlation graphic.

The equation almost perfectly identifies the lag, that was supposed to be 0.02 s, and it is shown as 0.025 s. To be noted, that the signals are real logged signals

from testing and the delay is not perfect, due to natural irregularities. With this method a problem can be solved. This identified the delay of the controller between the FCS command and the actual final command, that is the summation of the FCS and excitation value, seen in Figure 2.9.

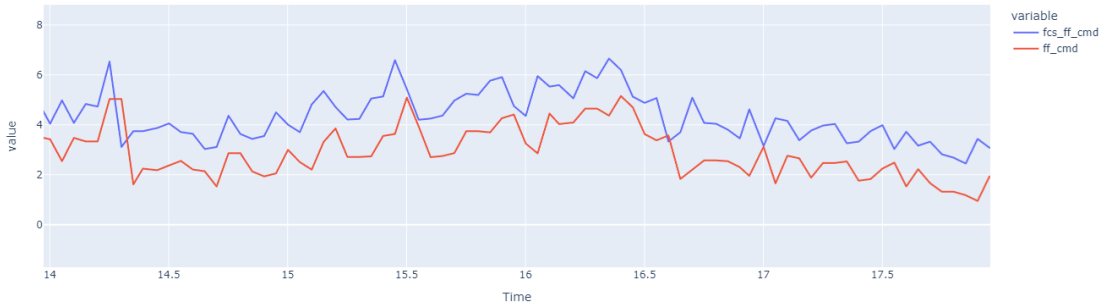

Figure 4.5: Forward flap transmitted command (ff_cmd) with a 20 ms delay relative to the command computed by the flight controller (fcs_ff_cmd)

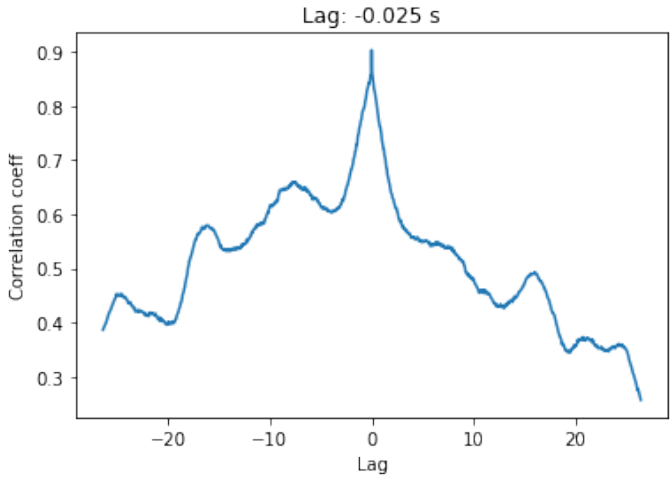

Figure 4.6: Cross-correlation and time delay graphical representation

4.5.4 Sampling Frequency

When selecting the sampling frequency it is important to take into consideration some aspects. First of all, the sampling frequency needs to be high enough to capture the important dynamics of the system without distorting them, phenomena known as aliasing, and not too high to respect the sensors limits and to avoid the gathering of unwanted noise that usually occurs in higher frequencies.

When considering the minimum sampling frequency, it is not enough to define it as the higher frequency the user wants to capture, neither by the Nyquist frequency, shown in equation (4.36), defined as the theoretical minimum sampling frequency to capture discrete samples of continuous signals with a frequency up to the f_s. This because aliasing can happen, where the captured signal is not defined by a sufficient number of points. In Figure 4.7 a sin wave with a frequency of 1Hz captured with

a sampling frequency slightly above f_N is represented. The sin wave is stretched by the sampling process and its frequency diminished [25].

$$f_N = \frac{f_s}{2} \tag{4.36}$$

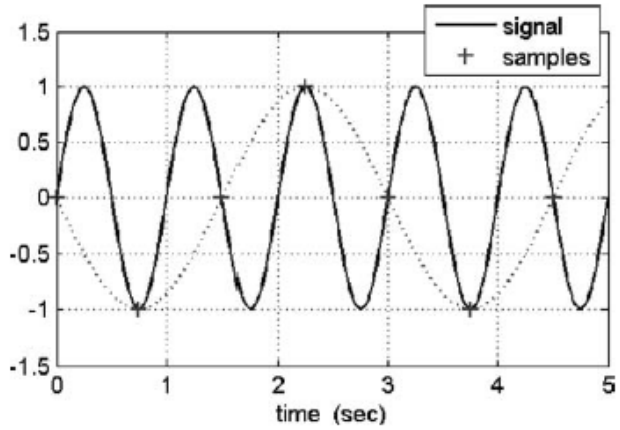

Figure 4.7: Aliasing example [25]

In practice, to obtain good results, considering f_{max} the maximum frequency of interest, f_s should be [25]

$$f_s = 25 f_{max} \tag{4.37}$$

With that being said, a first excitation of the system should be performed in order to understand where the most predominant frequencies are situated in the spectrum and decide an optimum f_s. When defining the input design, this is going to be calculated through the frequency transformation of the time response. From the results gathered from the initial tests, the predominant frequencies of the boat's dynamics were around 1-3 Hz, so a sampling rate of 100 Hz was tested, to have a safety margin.

4.5.5 Input Design

To properly identify a system, its dynamics need to be fully described in the data, in which the methods are acting upon. As it is usually said, it is impossible to identify something that is not there, and even if the identification looks correct it is going to fail when the parameters are subjected to validation data because most likely, this data is going to reflect the dynamics of the system differently [20].

Different maneuvers are needed to excite the different axes of the dynamic motion of the vessel. Since the longitudinal motion of the hydrofoil is being considered, the most important dynamics are related with the height, pitch and speed variations, function of the activation of the actuating surfaces (forward flap and and aft flaps). The aft flaps (starboard and port) are not going to be commanded individually or differentially in order to avoid excessive roll of the boat and other transverse movements. For that reason the aft flaps are actuated in an average command. Also both these actuations need to be orthogonal or uncorrelated not to mislead

the identification and associate different variations of the boats states to the same inputs. That is why these control surfaces are actuated within a time difference, enough for the boat to stabilize in between excitaions.

To ensure that the first paragraphs are fulfilled, tests were conducted for arbitrary inputs that could cause a general excitation of the dynamics, allowing for an initial glance at the data and analysis of the relevant factors to consider. After the data was recorded, it was possible to examine its frequency components to determine which frequency band was dominant and had the greatest impact on the outcomes.

As it was expected and shown in Figure 4.8, most of the predominant frequencies lie in the range of]0,3] Hz. From this point there are many ways to define the inputs required and some of them can be seen in references [20][33][36]. Some of the most common are: frequency sweeps, pulse signals, steps, doublets, 3211 signals, etc.

These different input signals can be employed in a variety of situations. Square waves have a broader frequency range that includes critical intermediate frequencies. That is why, in this report, only the steps, doublets and 3211 signals are studied, since they combine simplicity with good identification data.

When deciding which signal/combination of signals to choose, one key part to understand, is which frequencies of the system are going to be excited and if these ones are the ones required. Figure 4.9 is useful to understand the frequency components of the input signals defined [20].

Starting by the step input, it is interesting to understand that only the low frequencies of the system are going to be excited. The step function is of zero frequency however in the frequency domain is going to be a combination of sine waves of low frequencies. Also important to notice that as the Δt (step duration) increases its frequency shape gets narrower, increasing the energy of the lower frequency components and decreasing the energy of higher frequencies. The inverse happens with the decrease of Δt. The step input, can be useful to excite lower frequencies of the system, that usually are the ones of most importance for systems like the one in study. However the band range is really small limiting the dynamics in question.

Next the doublet input, consisting of one pulse excitation followed by its symmetric, almost like an approximated squared sine wave. It is characterized by its frequency (cycles per second), amplitude and by being symmetric in relation to the origin, useful to get the boat back into steady conditions. The doublet takes into consideration a broader frequency band than the step, where the frequency of the doublet is predominant with a quasi-linear attenuation of energy in nearby frequencies.

Finally the 3211 signal, where Δt is the duration of the smaller 1 pulses preceded by a $3\Delta t$ and a $2\Delta t$ pulse. This standard input can be really useful, since it broadens the spectrum of frequencies to which the system is going to react, as it can be seen in Figure 4.9. The downside is the asymmetry presented in this excitation, where, in the end, the boat has been excited more for the positive direction than the negative taking longer to settle into a steady condition. In the system of study this does not present as a problem, due to the fast control reaction and achievement of the steady state, also a time interval between excitations is given for this condition to be met [20].

With that being said for this specific report, initially, a combination of the step input and the 3211 signal is used. The 3211 signal alone would not be enough due to the fact that lower frequencies would be neglected and in this case they

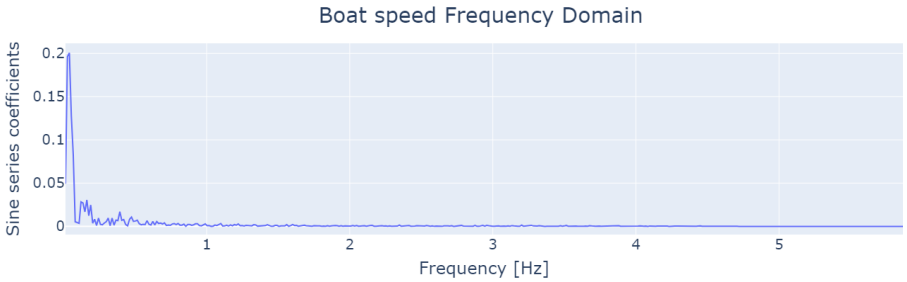

(a) Boat Speed

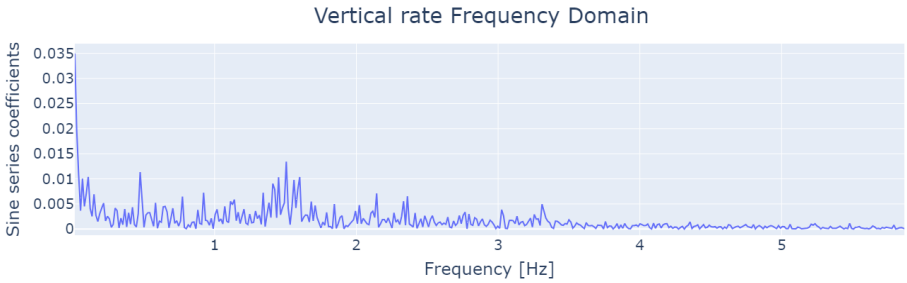

(b) Vertical rate

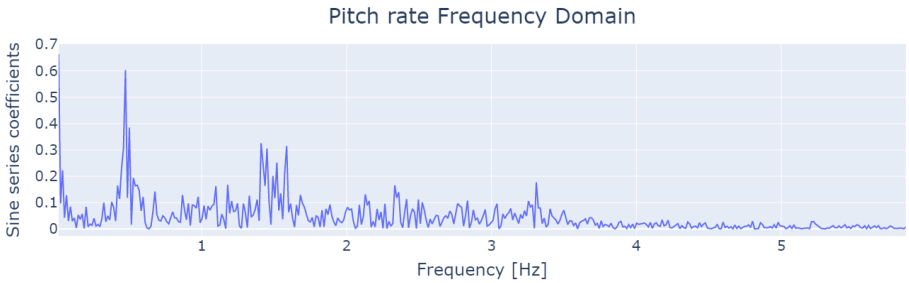

(c) Pitch Rate

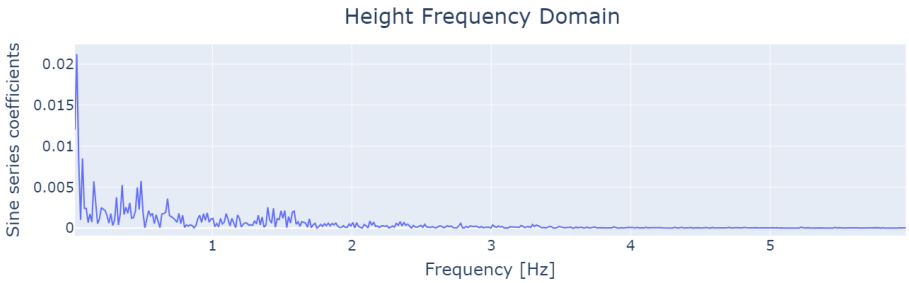

(d) Height

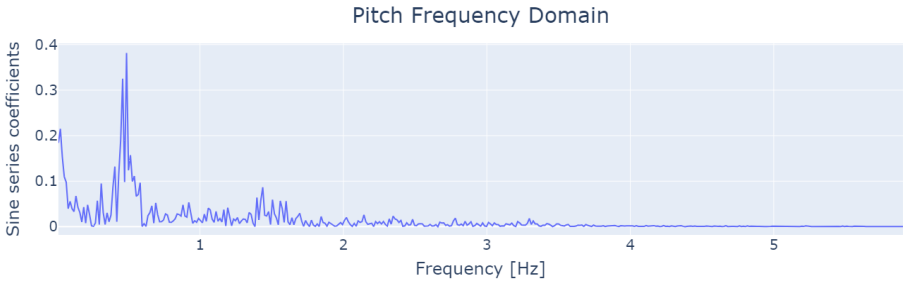

(e) Pitch

Figure 4.8: Frequency response of the system's states

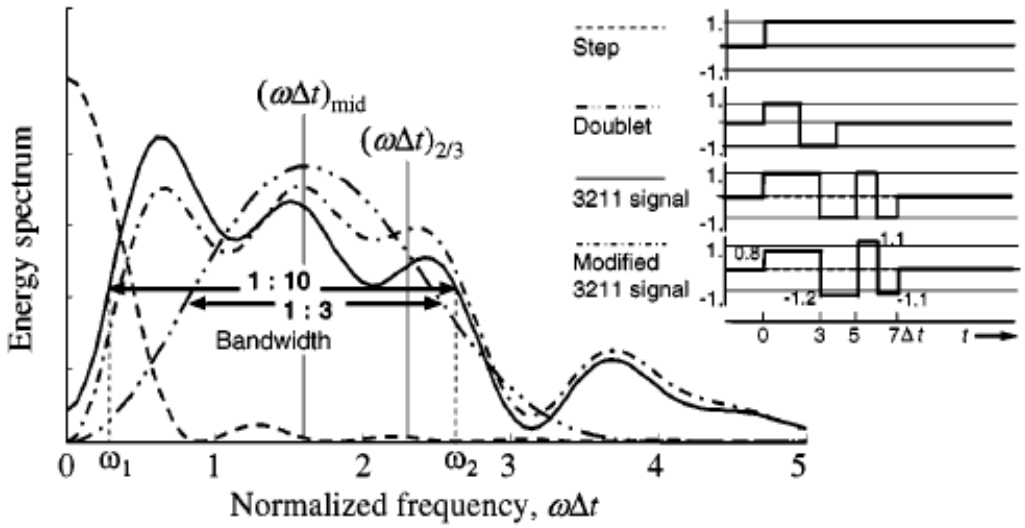

Figure 4.9: Energy spectrum of standard inputs [20]

are clearly relevant. Applying the step alone would cause the same deficit but in higher frequencies. All in all a combination of the two inputs would give the optimum excitation. This combination was applied to both actuating surfaces with a separating time interval, to ensure the orthogonality between excitations. The final excitation selected can be seen in Figure 4.10.

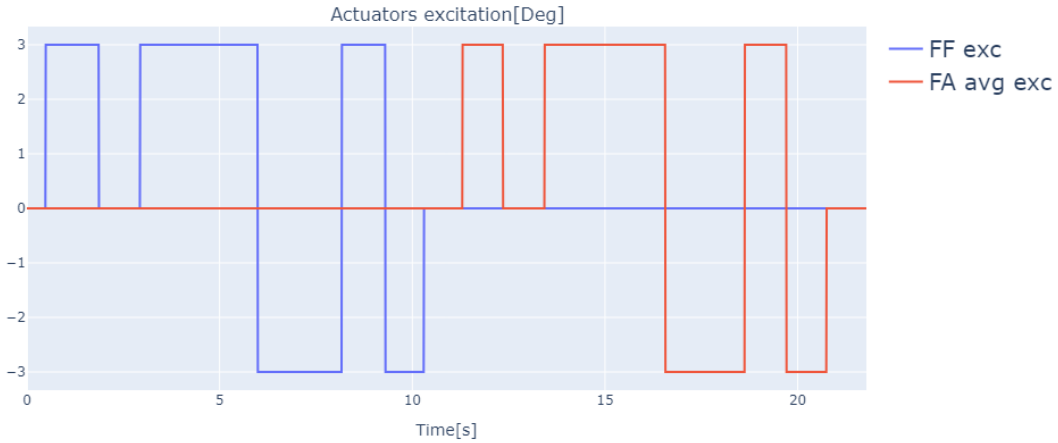

Figure 4.10: Forward (FF) and aft (FA) flap excitation signals

To apply this excitation both in real implementation and simulation data, a function was developed to be implemented in the software FaRo. This function was created according to the structure of the software being worked on with the objective of providing the capability of exciting the system with different signal structures.

It had as inputs the type of excitation (single step for one actuator, one step for each actuator, 3211, predefined square + 3211 with forward and aft flaps uncorrelated excitation,), amplitude of the signal, the actuator to which the excitation corresponds, the duration of the excitation corresponding to the "1" pulse in the

3211 signal or the step in the simple step signal, total excitation time, initial delay time of excitation, the time step of the software simulation cycles for the outputs to be time consistent, two binary flags one for turning on/off the excitation and other for turning on/off the automatic controller. The latter flag was developed for simulation purposes mainly, since operating hydrofoil vessels without automatic control can be dangerous due to the instability of the system. The outputs, as it is clear in Figure 4.10, are the command of the forward and average aft flaps amplitude of the vessel. The outputs can be changed according to the boat being worked on and its inputs. Finally this function automatically generated logs to store the data for future analysis.

4.6 Simulation Data

After having an understanding from the identification methods in the theoretical application, Section 4.2, these were applied to simulated data. Simulation data from FaRo offers information that could not be obtained in the theoretical evaluation, this because

- In FaRo the actual controller is implemented and is acting upon the inputs and outputs created.
- The data processing is the same that the boat experiments.
- It was possible to prepare the future implementation of this methods in real boats

Simulation data from the FaRo software was generated through the input function created and logged automatically.

In initial iterations the results were not satisfactory as the dynamics were not being excited properly. The fitness results were good for a first identification but the validation data was giving negative results. Also the results were worse when comparing with the theoretical fitness values determined before the simulations. It was noted that speed was not being excited, since it had close to no variation. Also the theoretical excitation had a faster excitation rate exciting faster dynamics of the vessel. To properly identify the system the dynamics being excited need to be the ones predominant in the regular usage of the boat.

With that being said two possible solutions were thought.

- Use motor thrust as input by changing its constant manually. The automatic control of the thruster is not implemented in the software yet so it cannot be considered as an input but as an external disturbance.
- Implement faster excitations with smaller time duration.

Applying random thruster excitations was not successful. It should work if it is considered as an input for the automatic control and that is going to be referred in the "Conclusions and Future work" section.

Bear in mind that the excitations mentioned for the FF and FA Avg are of the form of $step + 3211$ defined previously.

Faster excitations, with a $1\Delta T$ of 0.3 s versus the slower 1s were implemented, and their output results can be seen in Figure 4.11, for the identification data and in Figure 4.12 for the Validation data. Also, the fitness results for each output were evaluated. These results are shown for both identification and validation data. To notice, that the validation data is the same for both fast and slower excitaions.

Tables 4.15 and 4.16, show the fitness results for the slower excitation and for the faster excitation, respectively. It is shown, that the identification fitness for the slower excitation is superior to the one of the faster excitation. However, the overall fitness of the validation data, for a faster excitation, is higher than for the slower excitation.

A faster excitation alters the state of a system more abruptly, hence stimulating more the dynamics of the system. This can translate in matrices that represent the system better for different conditions and environments.

A slower excitation, stimulating slower dynamics, easier to identify, translates in a system that corresponds adequately to the momentary conditions. Yet, it misses to incorporate the overall dynamics of the boat and does not suit as well in other conditions than the ones used for the identification.

Figure 4.11: Org Vs. 1State Identification. "sim" represents the simulated data, "Org" the original non manipulated matrices and "1State" the manipulated matrices discussed in Section 4.2.3

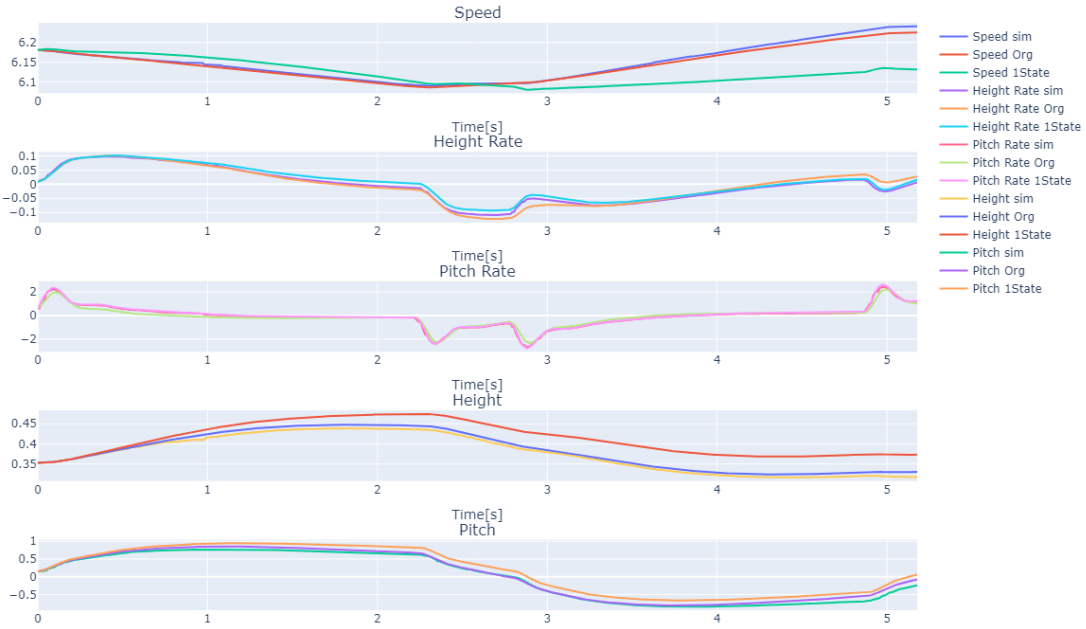

Figure 4.12: Org Vs. 1State Validation data.

	Fitness Org	Fitness Org Valid	Fitness 1State	Fitness 1State Valid
Speed	97.0260	-6.6553	91.0469	-23.7942
Height Rate	93.3250	78.0762	92.0225	81.3400
Pitch Rate	88.1254	87.0078	94.5019	92.5396
Height	96.5337	21.9829	84.3305	-0.7515
Pitch	96.4135	73.1544	95.2005	69.4106

Table 4.15: Simulation fitness results [%] for slower excitation. Valid stands for Validation data, 3rd and 5th columns. 2nd and 4th columns represent the identification fitness values. Same applies for Table 4.16.

	Fitness Org	Fitness Org Valid	Fitness 1State	Fitness 1State Valid
Speed	28.9463	84.762	41.6644	-17.1193
Height Rate	82.6095	80.2556	89.7541	82.9075
Pitch Rate	82.4554	78.8144	92.8323	92.7699
Height	27.539	83.3675	48.0845	12.2823
Pitch	81.2158	89.4507	86.5515	72.5661

Table 4.16: Simulation fitness results [%] for faster excitation

4.6.1 Speed Identification

Speed identification is expected to be more difficult since it mostly depends on the motor's thrust forces. With that, even with fast excitations on the actuators the boat's speed will not change abruptly, hence its dynamics are not going to be captured. The best solution would be to considered it as an input of the system, however the current software does not have this function implemented in the control system. In Section 6.2 a solution to implement speed as an input is discussed.

With real data, speed will be affected by other phenomena not considered for simulation purposes like the interactions with the ocean currents and waves, speed, etc. making possible to identify its dynamics.

4.6.2 Application of Identification Metrics

Using values from the identification of a real data set and after analyzing them graphically, it was concluded that the fitness of a given variable not always corresponds to a truly bad identification.

Figures 4.13 and 4.14 illustrate this point accordingly. It is possible to see that the identified speed curve is not matching the original values, however the difference is minimal relative to its maximum value and the RE (equation (4.20)) along time does not go above 2% even though its values of fitness are negative.

To further confirm this affirmation in Figures 4.15 and 4.16 the same process is done for the Pitch state for the same data set. Even if the Pitch fitness corresponds to a value of around 70 %, its relative errors can be as high as 30 %. Meaning that both curves are similar, having areas of almost null error, but in areas of abrupt changes the errors can achieve higher values. The user must know if these errors are allowable.

The RMSE (equation (4.21)) can be a good value to have as a reference of an average error along a data set, giving the user a notion of how much the predicted

state is deviating in absolute values of the reference state [47]. In Figure 4.13 the RMSE has a value of 0.061 knots while the mean speed fluctuate around 5.7 knots thus being a marginal error. However the RMSE for the Pitch fitness is of 0.1844° while this variable fluctuates around 0.5°. In this case the RMSE is not marginal and it needs to be taken into consideration.

In the end the RE indicates a relative percentage difference between curves, having the power of minimizing the relevance of fitness if it is proved that the RE is insignificant. The RMSE is related to an average absolute error along the data set so that the user realizes if that absolute value is critical. Analyzing maximum errors also indicates if the states are surpassing critical values, however, anti-windup systems are responsible of limiting such instabilities and if the system is proven as stable it should not happen.

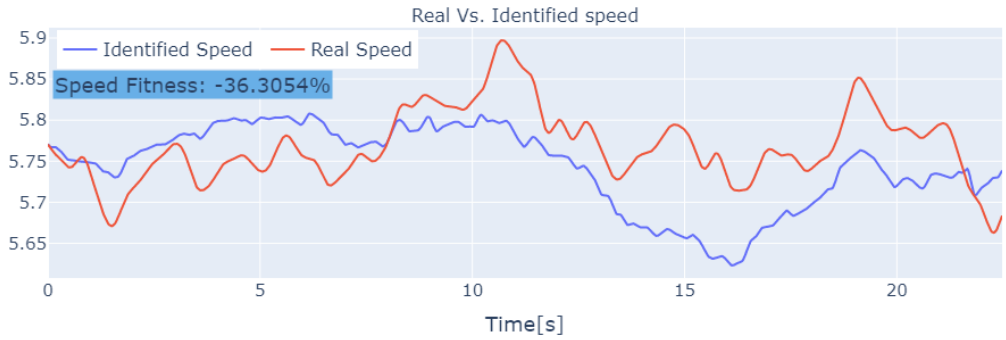

Figure 4.13: Real and Identified speed.Speed fitness between the two signals as an annotation

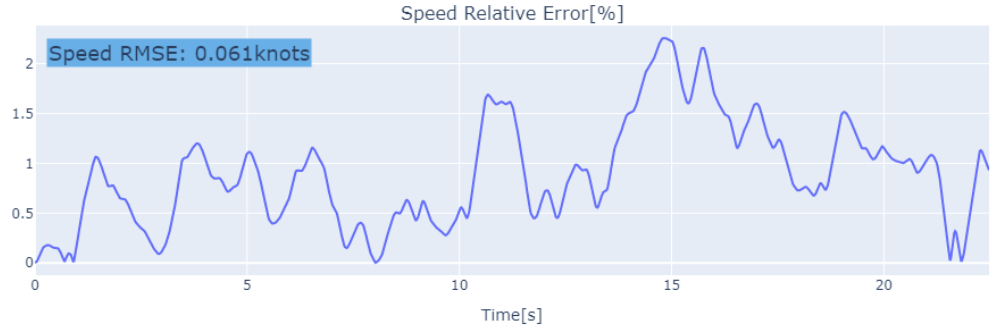

Figure 4.14: Speed identification RE and RMSE

Error and Fitness analysis needs to be interpreted by the user. Fitness values can be trusted when they overcome the 85%, 90% barriers since the fit is almost perfect and the errors are close to null. As it was seen for 70%, the highest achieved for the given data, it is still possible to have high percentual errors between curves,

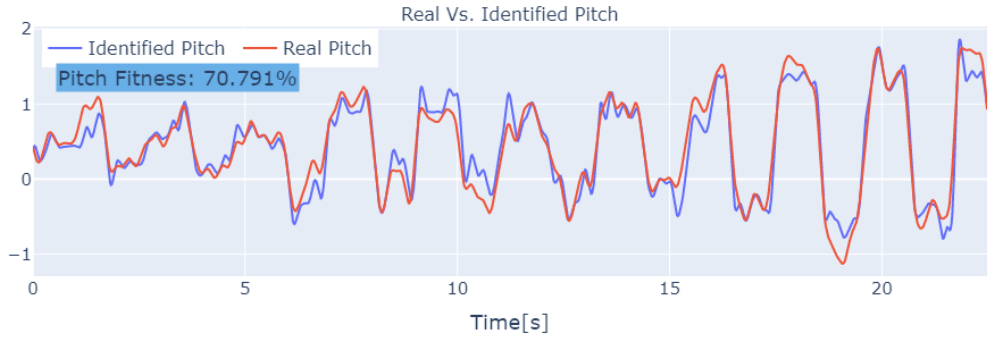

Figure 4.15: Real and Identified pitch.Pitch fitness between the two signals as an annotation

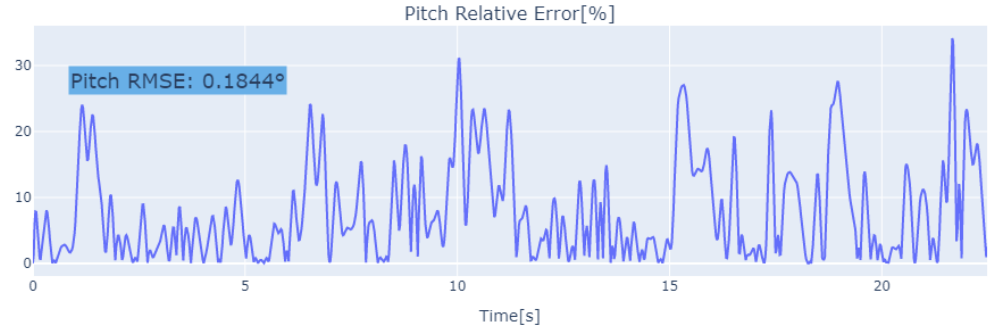

Figure 4.16: Pitch identification RE and RMSE

even if for a big part of the time interval the curves fit seamlessly. In future works (Sec. 6.2) an overall metric is referred as an interesting project.

Control Performance Metrics

There are numerous ways someone can model a system and develop a controller to it, in the end, there needs to be a set of criteria that distinguishes each pair of model/controller and determines if it is performing accordingly. In this section the performance metrics utilised to evaluate the success of the controller associated with the system identified previously are displayed.

5.1 Phase and Gain Margins

The first step to understand if a system is stable or not should be to compute the system's open-loop and closed-loop poles, in order to confirm the existence of poles in the right-hand side of the imaginary plane. However, these poles are part of an user-determined system's dynamics and control matrices, not taking into account the full spectrum of unpredictable phenomena. This means that the poles that are being analyzed come with an associated uncertainty and do not reflect the complete nature of the system. Furthermore, like most of engineering problems, a margin should be set to guarantee a safety gap between stability and instability.

Phase and gain margins are one of the simplest methods to evaluate how close a stable system is of being unstable. These take as a premise that the closed loop system is unstable if one frequency produces 0 dB gain and -180° phase. The most direct method to compute these margins is through the Bode plot analysis.

The gain margin dictates how much can the gain be increased until the system is unstable and is determined at the phase crossover frequency, when the phase angle of the open-loop transfer function is -180°.

The phase margin dictates how much additional phase lag can be added at the gain crossover frequency (0 dB), until the system becomes unstable. It is given by the phase angle of the open-loop transfer function at the gain crossover frequency plus 180°.

Figure 5.1 depicts how these margins can be calculated and reflects another key point for detecting if a system is stable or unstable from the get go. If the phase or the gain margins are negative the system's instability can be assumed [40].

Even though these metrics can be important to perform an immediate analysis of the system's stability they can be insufficient due to the fact that they do not take into account simultaneous variation of gain and phase for a specific transfer function. Also, for MIMO systems phase and gain margins determine the stability for a 1 to 1 relation between a given input and output. This means that we cannot be sure if a system is stable for 2 changes at the time just by looking at the Bode plots due to the existent correlations in between states and inputs.

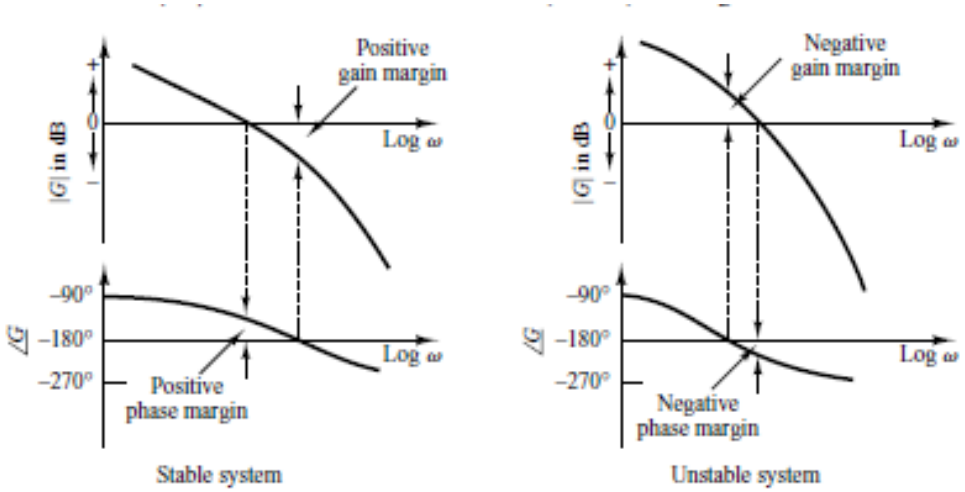

Figure 5.1: Gain and phase margins of a stable(left) and unstable system(right) [40]

5.2 Robustness - Disk Margins

By looking at a a stable system's Bode plots we can commit the error to assume that a system is stable, for various reasons, listed below:

- Mathematical models do not represent a system's dynamics 100% accurately and its transfer functions gains and phase can differ from what was determined.
- Bode plots only represent the stability for a single gain or phase uncorrelated changes and for the relation of one input to another. Simultaneous gain and phase changes for multiple inputs/outputs are not taken into consideration. The "loop-at-a-time analysis" does not encompass multiple perturbations in different inputs and outputs.
- Sensitivity of a system is not analyzed. A system with a big gain and phase margins, apparently stable, can be sensitive to small simultaneous gain and phase margins by having a Nyquist curve approaching -1 [24].
- Margin requirements need to take into account increase of uncertainty at higher frequencies.

For a better robustness analysis of a feedback system, for this report, Disk margins were computed as to evaluate a system's stability for different gains and dynamics matrices [24].

Describing disk margins, as succinct as possible, they consist of a set of perturbations corresponding to a gain and/or phase variation to which the system remains stable. These disks or sets of perturbations can be computed for a single input or output or for multiple inputs and outputs, being the more generalized result given by the disk that takes into account the entirety of the input/output correlations [49].

Each set of perturbations is represented as $D(\alpha, \sigma)$, a disk which parameters correspond to the maximum size (α) for which the closed loop maintains stability for a given skew (σ). These perturbations represent the uncertainties of the model

that was developed, ensuring these stability margins guarantees that the model's inaccuracy does not deviate into unstable conditions [49].

Figure 5.2, represents a system's closed-loop with a perturbation, f, to a plant, P, with a controller, K, integrated in the diagram.

Looking at Figure 5.3 it is easier to understand how the disks parameters interact with it and what do they represent. The skew (σ) is defined according to the user's perception of how the gain is more likely to vary according to the system uncertainty. If the user believes that the real system will have gains bigger than the ones predicted, a more positive skew will encompass points which the gains will be higher and vice-versa. In this case of Figure 5.3, the skew is zero since there is the belief that the model is accurate or the user does not know whether the gain is likely to be higher or lower. Also, it is important to notice that as the skew increases or decreases so does the phase margin, in this case. (α) is calculated for a given skew and and will be a measure of the size of the disk that will encompass all the stable perturbations represented by the green dots. Each dot is a complex number representing a perturbation to a system.

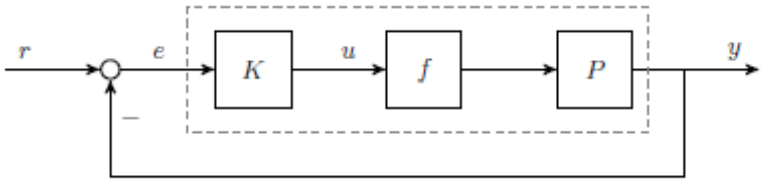

Figure 5.2: Feedback loop with a perturbation f [49]

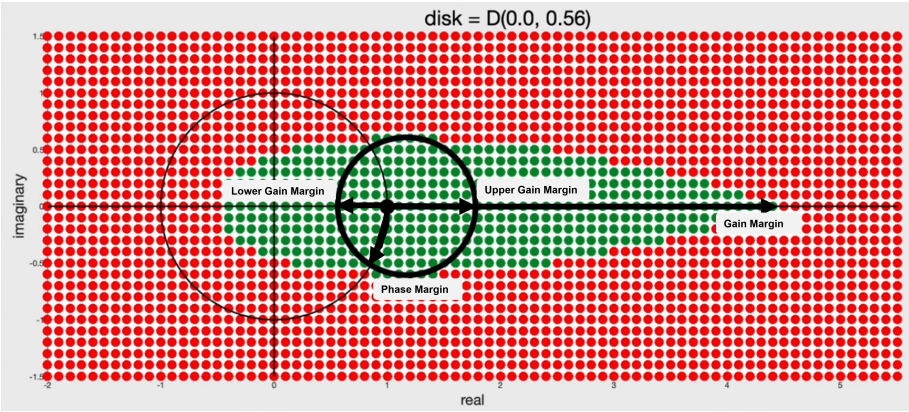

Figure 5.3: Disk margin for a given system (adapted from [31])

By looking at Figure 5.3 it seems that this metric can be a little conservative since the pure gain and phase margins are higher than the upper and lower disk gain margins (phase margins are symmetric and for zero skew disk and traditional phase margins coincide). However for higher increases of the gain, little phase variations will get the system to be unstable.

Finally, one of the most important points to retain is that, through the Robust control toolbox from Matlab, it is possible to compute MIMO disk margins that take into consideration the presence of perturbations for every channel of the feedback closed-loop (inputs and outputs) simultaneously and establish the final gain

and phase margins for the system, as a whole. This is extremely useful for the optimisation of the gain matrix to place the closed-loop poles of the system in the left-hand side of the imaginary plane while maintaining stability and performance with a comfortable margin.

In Figure 5.4 it is possible to identify a disk margin plot for the closed loop system of the theoretical global system shown in equation (4.18). The gain and phase margin are computed from the simultaneous variations of the inputs and outputs of the system. In the case of this system, the gain and phase margins can vary according to the points that belong to the disk area, in order to maintain stability.

It is also possible to analyze if it is worth it to skew the disks and if the system is more stable for different sets of gains. Skewing the system by a σ of 2 turns it into a less stable system by having a smaller disk margin in every axis, as it is depicted in Figure 5.5.

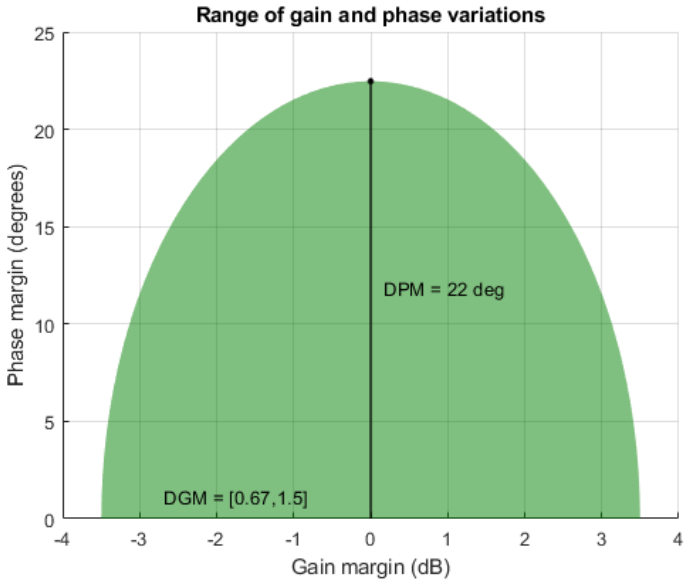

Figure 5.4: Disk margin from theoretical matrices

In the end the goal is to be able to compare different system's dynamics stability and access which one fits better in the requirements.

5.3 Errors

Besides analyzing the fitness of the identified matrices, calculating the root-mean squared error (RMSE) and the relative error (RE) can also be an important measure to analyze if the system is following the reference values and performing as desired. These can be applied to the controlled states and commands to evaluate the control system tracking stability, precision, and accuracy, providing important control performance feedback. The fact that these metrics can be easily computed in real-time is also very important.

These error metrics were already introduced in section 4.3 and are already implemented in the FaRo software being of great importance for performance analysis.

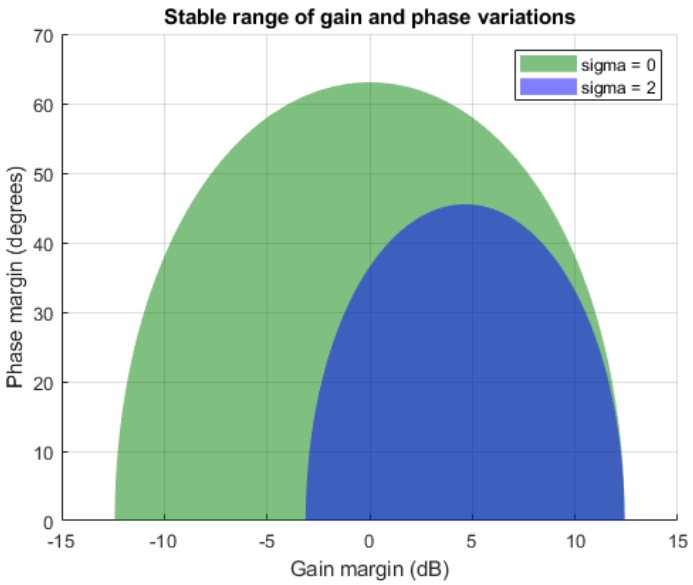

Figure 5.5: Disk margin for $\sigma = 0$ and $\sigma = 2$

5.4 Proposed Performance Evaluation Methodology

In the previous 2 chapters a system identification and performance metrics analysis methodology was introduced. Even though the objective was for these topics to be applied in real data, that was not possible. A brief summary of the final process for optimizing the hydrofoiling controller is now presented.

The first step is to gather sufficient data to have proper identification of the system's dynamics. FaRo software alongside with the boat's sensors have the capability of collecting data at 100 Hz and, with the new function developed, to excite the boat's actuators with steps and 3211 signals.

After the logs are collected it is important to analyze the inputs and states frequency contents to determine to which frequency the filters should be implemented. Also the identification of outliers and time delays should be done alongside the frequency analysis. The quality of the data pre-identification should be ensured.

The third step involves applying the different identification methods ('N4SID', 'MOESP', 'PARSIM-K') to the already treated data. As discussed before these methods can be applied to the original data (5 states) or to the modified data (3 steps) to constrain the identification in maintaining the equality between outputs and inputs for the pitch rate and height rate.

A set of metrics is then used to determine if the identification was successful and if the identified matrices actually represent the real system better than the theoretically matrices. For the new dynamics closed-loop matrices the open-loop matrices can be computed by subtracting a product of B and K. This is important to use the Matlab functionalities of the Robust Control library and develop the disk margins. These margins need to be enough for the system to be stable for different conditions, if not K can be manipulated in order to reposition the system's poles and ensure stability. Another way of changing the system's poles is through an LQR algorithm in which, by defining weighting matrices for performance and for control,

optimized K values are determined.

Finally it would be interesting to implement the new controller gains and analyze the performance differences. This final structure is represented in a diagram in Figure 4.3. Last conclusions and future work are explicit in chapter 6.

Conclusions and Future Work

6.1 Conclusions

This report provides a full process of identifying real model parameters, from the treatment of logged test data, going through the identification algorithms to its evaluation through different metrics.

Firstly, in Section 2.1, the reader can understand the historical evolution of hydrofoil boats and why they can be an emerging technology of the future. Its innovations and advantages compared with traditional vessels are clear. These include, the comfort of traveling by avoiding wave collisions and oscillations; energetic efficiency, offering the possibility of sustainability by electrifying marine transportation and reduced levels of environment and sound pollution.

Furthermore, developments on hydrofoil implementation are being made with companies pushing for its commercial implementation. Geometric, dynamic and control models are shown proving the in depth knowledge present in this area, as it can be seen in Section 3.2.

Besides the theoretical knowledge, in this work, a methodology for the symbiosis between theory and practice is shown. Through system identification algorithms, such a N4SID, MOESP and PARSIM-K, it was shown, in Section 4.2 that it is possible do identify a model's parameters successfully from sampling rates of 100 Hz, which is feasible to have in real logging systems. This success was achieved through applying these algorithms to the different closed-loop dynamic theoretical matrices, these being, the vertical, horizontal, vertical + horizontal, angular and global dynamics. A fitness metric was used to evaluate the performance of the identification algorithms, and it was soon concluded that they were applicable for different conditions. N4SID and MOESP were the most promising ones showing good results for 100 Hz data and above, considering the original data. PARSIM-K showed to be better when the inputted data was manipulated, in order to apply constraints in some parameters, to represent states that are time integrations of others. The non-manipulated data gave better results overall.

To reinforce the applicability of the identification algorithms, these were used in simulation data gathered from the FaRo software simulator, in section 4.6.

For the application of these methods to real logged data from hydrofoil tests, some methodologies of data processing were discussed. In Section 4.5.2, noise analysis of data sets in the frequency domain was performed. It consisted in different equations, alongside with visual aid, to determine the optimum cutoff frequency to which a 4th order Butterworth Filter was applied. This operation was done successfully, since the identification of a data set proved to be much better after noise

elimination. Signal delay observations, in Section 4.5.3 were also made, through cross-correlation functions, and exhibited the existence of delay in the samples. Finally, in the data processing section, an ideal input design was developed to collect high quality information for system dynamics identification, by exciting the most important frequencies. This design consists in a step + 3211 signal, described in section 4.5.5, that broadens the frequency spectrum of the excitation, for a given time sample interval.

Lastly, different performance and stability metrics were applied, such as, phase, gain and disk margins, RMSE (Root Mean Square Error) and RE (Relative Error). Disk margins manifested to be more complete than phase and gain margins, because of the fact that these take into consideration all the correlations between each input and output of a MIMO system. Also, disk margins, provide results to simultaneous gain and phase variations instead of individual changes and offer an important view of how the system is going to remain stable and which deviations will make it unstable, these were discussed in Section 5.2. RE and RMSE are helpful in determining the relevance of the fitness results. One should take into consideration both sides of the evaluation (fitness and errors) to have the complete set of information to determine the success of the identification, as it was described in Section 5.3.

In the end, a complete methodology, summarized in Section 5.4, was developed to properly identify a hydrofoil boat dynamics.This allows to determine if the identified closed-loop matrix, along with the gain matrix, are stable and performing as desired. Unfortunately it was not possible to apply this methods to a complete set of real data due to unexpected unavailability of test vehicles.

6.2 Future Work

Theoretical definition of a system's dynamics appears to be insufficient since it does not reflect reality 100%. It would be interesting to apply all the gathered knowledge in real hydrofoil boats testing and tuning. That way, through the performance metrics defined, it would be possible to understand where the process and the control of a system can be improved.

A second step could be to implement automatic control gain tuning using real-time system identification and evaluation of an object performance. The methodology defined throughout this report could be useful, since it provides useful identification algorithms and metrics to evaluate its performance. Also an overall control performance metric, combining the ones described could be developed.

Thirdly, implementing thrust as an input to the model could be advantageous. Introducing thrust step excitations to the system would provide another tool to improve the quality of identification data.

Finally, a speed estimator could also be added. There is an indirect relation between the motor rpms and the boat speed, since a change in the motor velocity will affect the boat speed differently at different velocities. This ends up being an indirect measurement of the ocean movements due to the fact that we are interested in the relative speed between the motor and the water. GPS information is not enough due to the water currents. Experimental testing can be done to determine this relation.

Bibliography

[1] Hirotugu Akaike. "Canonical Correlation Analysis of Time Series and the Use of an Information Criterion". In: *System Identification Advances and Case Studies*. Ed. by Raman K. Mehra and Dimitri G. Lainiotis. Vol. 126. Mathematics in Science and Engineering. Elsevier, 1976, pp. 27–96. DOI: https://doi.org/10.1016/S0076-5392(08)60869-3. URL: https://www.sciencedirect.com/science/article/pii/S0076539208608693.

[2] *America's Cup*. URL: https://www.americascup.com/.

[3] J.D. Anderson. *Aircraft Performance & Design*. McGraw-Hill international editions. McGraw-Hill Education, 1999. ISBN: 9780070019713. URL: https://books.google.pt/books?id=PwtO7aiwbBwC.

[4] Giuseppe Armenise, Marco Vaccari, Riccardo Bacci di Capaci, and Gabriele Pannocchia. "An Open-Source System Identification Package for Multivariable Processes". In: (Sept. 2018), pp. 152–157. DOI: 10.1109/CONTROL.2018.8516791.

[5] Ricardo Bencatel, Smrithi Keerthivarman, Ilya Kolmanovsky, and Anouck Girard. "Full State Feedback Foiling Control for America's Cup Catamarans". In: *IEEE Transactions on Control Systems Technology* PP (Jan. 2020), pp. 1–17. DOI: 10.1109/TCST.2019.2955059.

[6] Ricardo Bencatel, Fabrizio Marabini, and Roberto Berrozpe. "Boats Dynamics Models". 2021.

[7] ACE / Studio Borlenghi. *36th America's Cup Day 7: Luna Rossa Prada Pirelli*. 2021. URL: https://www.sail-world.com/news/236712/Americas-Cup-Luna-Rossas-control-systems-outed.

[8] Alain J Brizard. *Introduction To Lagrangian Mechanics, An*. World Scientific Publishing Company, 2014.

[9] J.S. Carlton. "Chapter 12 - Resistance and Propulsion". In: *Marine Propellers and Propulsion (Fourth Edition)*. Ed. by J.S. Carlton. Fourth Edition. Butterworth-Heinemann, 2019, pp. 313–365. ISBN: 978-0-08-100366-4. DOI: https://doi.org/10.1016/B978-0-08-100366-4.00012-2. URL: https://www.sciencedirect.com/science/article/pii/B9780081003664000122.

[10] Charles M Close, Dean K Frederick, and Jonathan C Newell. *Modeling and analysis of dynamic systems*. John Wiley & Sons, 2001.

[11] Kévin Colin, Xavier Bombois, Laurent Bako, and Federico Morelli. "Closed-loop identification of MIMO systems in the Prediction Error framework: Data informativity analysis". In: *Automatica* 121 (Nov. 2020), p. 109171. DOI: 10.1016/j.automatica.2020.109171.

[12] Rodriquez Consulting. *Hydrofoil Super yacht? The Birth of The Hyper Yacht*. 2019. URL: https://rodriquezconsulting.com/hydrofoil-superyacht/.

[13] R.C. Dorf and R.H. Bishop. *Modern Control Systems (thirteenth Edition)*. Dian zi gong ye chu ban she, 2018. ISBN: 9787121343940. URL: https://books.google.pt/books?id=x4TyvgEACAAJ.

[14] Odd M. Faltinsen. *Hydrodynamics of High-Speed Marine Vehicles*. Cambridge University Press, 2006. DOI: 10.1017/CBO9780511546068.

[15] *FaRo Advanced Systems*. 2022. URL: http://www.faroadv.com/.

[16] Richard Fitzpatrick. "Newtonian dynamics". In: (2011).

[17] Zoran Gajic. *Linear dynamic systems and signals*. Prentice Hall/Pearson Education Upper Saddle River, 2003.

[18] Slim Hachicha, Maher Kharrat, and Abdessattar Chaari. "N4SID and MOESP Algorithms to Highlight the Ill-conditioning into Subspace Identification". In: *International Journal of Automation and Computing* 11 (Feb. 2014), pp. 30–38. DOI: 10.1007/s11633-014-0763-z.

[19] I. W. Jamaludin, N. A. Wahab, N. S. Khalid, S Sahlan, Z. Ibrahim, and M F. Rahmat. "N4SID and MOESP subspace identification methods". In: *2013 IEEE 9th International Colloquium on Signal Processing and its Applications*. 2013, pp. 140–145. DOI: 10.1109/CSPA.2013.6530030.

[20] R.V. Jategaonkar. *Flight Vehicle System Identification: A Time-domain Methodology*. Progress in astronautics and aeronautics. American Institute of Aeronautics and Astronautics, Incorporated, 2015. ISBN: 9781523100804. URL: https://books.google.pt/books?id=lOLzjwEACAAJ.

[21] D. Jones and L. Kenny. "The design of the jetfoil". In: *Hovering Craft and Hydrofoil* (Oct. 1977).

[22] Rudolf E. Kálmán. "Contributions to the Theory of Optimal Control". In: 1960.

[23] Tohru Katayama et al. *Subspace methods for system identification*. Vol. 1. Springer, 2005.

[24] IS Khalil, JC Doyle, and K Glover. *Robust and optimal control*. Prentice hall, 1996.

[25] V. Klein and E.A. Morelli. *Aircraft System Identification: Theory and Practice*. AIAA education series. American Institute of Aeronautics and Astronautics, 2006. ISBN: 9781563478321. URL: https://books.google.pt/books?id=SC90QgAACAAJ.

[26] Emery Ku. "Modelling the human cochlea". In: *The Journal of the Acoustical Society of America* 126 (Dec. 2009), p. 3373. DOI: 10.1121/1.3270469.

[27] W.S. Levine. *Chapter 17-Linear Quadratic Regulator Control*. Electrical engineering handbook series. CRC Press, 2011. ISBN: 9781315218700. URL: https://books.google.pt/books?id=fX9ztgEACAAJ.

[28] L. Ljung. *System Identification: Theory for the User*. Prentice Hall information and system sciences series. Prentice Hall PTR, 1999. ISBN: 9780136566953. URL: https://books.google.pt/books?id=nHFoQgAACAAJ.

[29] Pedram Masajedi, Afshin Ghanbarzadeh, and Laleh Fatahi. "The Optimization of a Full State Feedback Control System for a Model Helicopter in Longitudinal Movement". In: *International Journal of Intelligent Information Processing* 3 (Dec. 2012). DOI: 10.4156/ijiip.vol3.issue4.2.

[30] MATLAB. *version 7.10.0 (R2010a)*. Natick, Massachusetts: The MathWorks Inc., 2010.

[31] Matlab. *Understanding Disk Margin — Robust Control, Part 2*. Apr. 2020. URL: https://www.youtube.com/watch?v=XazdN6eZF80&t=749s.

[32] John R. Meyer. *Ships that fly*. 1990.

[33] Murat Millidere. "Optimal input design and system identification for an agile aircraft". PhD thesis. Middle East Technical University, 2021.

[34] *Mobyfly*. 2022. URL: mobyfly.com.

[35] A.F. Molland and S.R. Turnock. *Marine Rudders and Control Surfaces: Principles, Data, Design and Applications*. Elsevier Science, 2011. ISBN: 9780080549248. URL: https://books.google.pt/books?id=6e%5C_mkgRPVkUC.

[36] Eugene Morelli. "Practical Aspects of Multiple-Input Design for Aircraft System Identification Flight Tests". In: Aug. 2021. DOI: 10.2514/6.2021-2795.

[37] Miguel Mujica Mota and Maurice Meche. "Towards a Greener Europe: Analysis of the SeaBubble waterline in Rotterdam". In: (Sept. 2021). DOI: 10.46354/i3m.2021.emss.038.

[38] USS Aries Hydrofoil Museum. *U.S. Navy FRESH-1 Hydrofoil*. URL: https://www.ussaries.org/us-navy-fresh-1.

[39] J. Nazarzadeh, M. Razzaghi, and K.Y. Nikravesh. "Solution of the matrix Riccati equation for the linear quadratic control problems". In: *Mathematical and Computer Modelling* 27.7 (1998), pp. 51–55. ISSN: 0895-7177. DOI: https://doi.org/10.1016/S0895-7177(98)00035-1. URL: https://www.sciencedirect.com/science/article/pii/S0895717798000351.

[40] K. Ogata. *Modern Control Engineering*. Instrumentation and controls series. Prentice Hall, 2010. ISBN: 9780136156734. URL: https://books.google.pt/books?id=Wu5GpNAelzkC.

[41] R.C. Panda. *Introduction to PID Controllers: Theory, Tuning and Application to Frontier Areas*. IntechOpen, 2012. ISBN: 9789535160984. URL: https://books.google.pt/books?id=TkXPzgEACAAJ.

[42] Gabriele Pannocchia and Mirco Calosi. "A predictor form PARSIMonious algorithm for closed-loop subspace identification". In: *Journal of Process Control* 20.4 (2010), pp. 517–524. ISSN: 0959-1524. DOI: https://doi.org/10.1016/j.jprocont.2010.01.004. URL: https://www.sciencedirect.com/science/article/pii/S0959152410000259.

[43] Martin Placek. *Ocean shipping worldwide - statistics facts*. 2021. URL: https://www.statista.com/topics/1728/ocean-shipping/#dossierKeyfigures. (accessed: 23.05.2022).

[44] Mohd Rahmat and Mohd Syakirin Ramli. "Servomotor Control Using Direct Digital Control And State–Space Technique". In: *Jurnal Teknologi* 49 (Dec. 2008). DOI: 10.11113/jt.v49.196.

[45] Sudhahar S, Ganesh C, and Sharmila D. "Closed Loop Subspace Identification and Control of a two input-Single output Conical Tank System". In: (Aug. 2020). DOI: 10.20944/preprints202008.0401.v1.

[46] R.D. Schachter and Gabriel T. Fonteles. "Preliminary design dimensioning of hydrofoil boats with fully submerged and surface piercing foils". In: *Mar Syst Ocean Technol* (Mar. 2022). DOI: 10.1017/CBO9780511546068.

[47] W. C. Schultz and V. C. Rideout. "Control system performance measures: Past, present, and future". In: *IRE Transactions on Automatic Control* AC-6.1 (1961), pp. 22–35. DOI: 10.1109/TAC.1961.6429306.

[48] *Seabubbles*. 2022. URL: https://www.seabubbles.com/.

[49] Peter Seiler, Andy Packard, and Pascal Gahinet. "An Introduction To Disk Margins". In: *IEEE Control Systems Magazine* 40 (Oct. 2020). DOI: 10.1109/MCS.2020.3005277.

[50] Emily Sesno. URL: https://manoa.hawaii.edu/sealearning/media_colorbox/4446/media_original/en.

[51] Matthew Sheahan. *Foiling: the history of the hydrofoiler*. 2022. URL: https://www.yachtingworld.com/features/foiling-the-history-of-the-hydrofoiler-135741. (accessed: 23.05.2022).

[52] Mokhtar Shouran and Elmazeg Elgamli. "Design and Implementation of Butterworth Filter". In: *International Journal of Innovative Research in Science Engineering and Technology* 9 (Sept. 2020), p. 7975.

[53] A.K. Tangirala. *Principles of System Identification: Theory and Practice*. CRC Press, 2018. ISBN: 9781439896020. URL: https://books.google.pt/books?id=aUHOBQAAQBAJ.

[54] Herbert Tulleken. "Generalized Binary Noise Test-Signal Concept for Improved Identification-Experiment Design". In: *Automatica* 26 (Jan. 1990), pp. 37–49. DOI: 10.1016/0005-1098(90)90156-C.

[55] Shyh-Kuang Ueng, David Lin, and Chieh-Hong Liu. "A ship motion simulation system". In: *Virtual Reality* 12 (Mar. 2008), pp. 65–76. DOI: 10.1007/s10055-008-0088-8.

[56] Peter Van Overschee and Bart De Moor. "N4SID: Subspace algorithms for the identification of combined deterministic-stochastic systems". In: *Automatica* 30.1 (1994). Special issue on statistical signal processing and control, pp. 75–93. ISSN: 0005-1098. DOI: https://doi.org/10.1016/0005-1098(94)90230-5. URL: https://www.sciencedirect.com/science/article/pii/0005109894902305.

[57] Peter Van Overschee and Bart De Moor. "Subspace identification for linear systems. Theory, implementation, applications. Incl. 1 disk". In: vol. xiv. Jan. 1996, pp. xiv + 254. ISBN: 0-7923-9717-7. DOI: 10.1007/978-1-4613-0465-4.

[58] Guido Van Rossum and Fred L. Drake. *Python 3 Reference Manual*. Scotts Valley, CA: CreateSpace, 2009. ISBN: 1441412697.

[59] Michel Verhaegen. "Identification of the deterministic part of MIMO state space models given in innovations form from input-output data". In: *Automatica* 30.1 (1994), pp. 61–74. ISSN: 0005-1098. DOI: https://doi.org/10.1016/0005-1098(94)90229-1. URL: https://www.sciencedirect.com/science/article/pii/0005109894902291.

[60] Donald F Young, TH (Theodore Hisao) Okiishi, and Wade Huebsch. *Fundamentals of fluid mechanics*. Wiley, 2006.

[61] Bing Yu, David Gabriel, Larry Noble, and Kai-Nan An. "Estimate of the Optimum Cutoff Frequency for the Butterworth Low-Pass Digital Filter". In: *Journal of applied biomechanics* 15 (Aug. 1999), pp. 319–329. DOI: 10.1123/jab.15.3.318.

Appendix A

Global Fourier Transform

The Fourier transform applied was based on information gathered from [25].

Considering a measured variable $z(t)$ sampled at intervals Δt for N time samples where,

$$z(i) = z(i\Delta t) \qquad i = 0, 1, 2, ..., N-1 \tag{A.1}$$

The objective is to transform data from the time domain to the frequency domain. For that, finite, discrete Fourier transform is going to be applied. This implies that the signals used are periodic, however most of the signals under consideration are not periodic, so transformations need to be done. The first step will be to subtract a linear trend and make endpoints values equal to zero. After that, the signal should be reflected about the origin to make it periodic. The new time history becomes $g(i)$ where $g(-N+1) = g(0) = g(N-1) = 0$. $g(i)$ becomes,

$$g(i) = z(i) - z(0) - i\left(\frac{z(N-1) - z(0)}{N-1}\right) \qquad i = 0, 1, 2, ..., N-1 \tag{A.2}$$

$$g(-i) = -g(i) \qquad i = 1, 2, ..., N-1 \tag{A.3}$$

In Figure A.1 the original data in the time domain is shown and in Figure A.2 data ready for the Fourier transform can be seen.

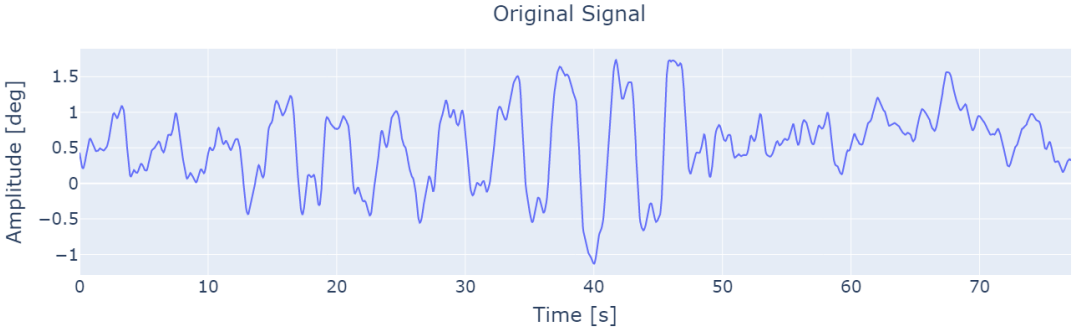

Figure A.1: Original Signal

expanding function g with a sine Fourier series,

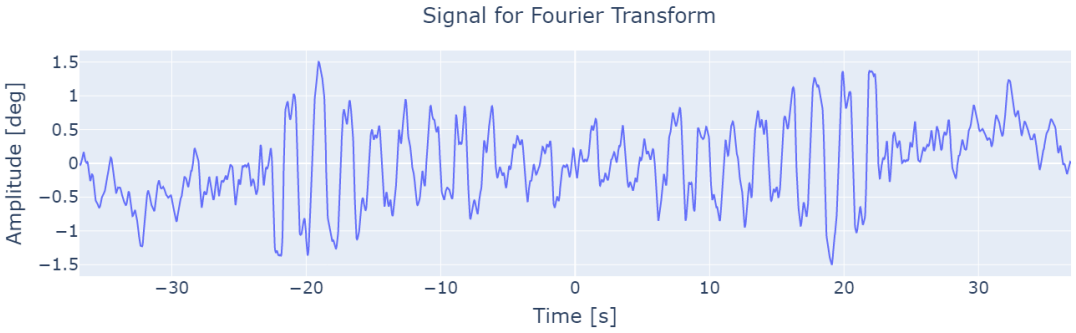

Figure A.2: Periodic signal with endpoint discontinuities removed

$$\hat{g(i)} = \sum_{k=1}^{N-1} b(k) sin\left[k\pi\left(\frac{i}{N-1}\right)\right] \qquad i = 0, 1, 2, ...N-1 \tag{A.4}$$

where $b(k)$ are the sine series coefficients and $\hat{(}g(i)$ is the approximation of $g(i)$ using Fourier sine series transformation. For this process only positive values of i were used, because they correspond to the original function. $b(k)$ is given by,

$$b(k) = \frac{2}{N-1} \sum_{i=1}^{n-2} g(i) sin\left[k\pi\left(\frac{i}{N-1}\right)\right] \qquad k = 1, 2, ..., N-1 \tag{A.5}$$

Each coefficient $b(k)$ corresponds to one frequency f_k related to index k by,

$$f_k = \frac{k}{2(N-1)\Delta t} \tag{A.6}$$

Figure A.3 illustrates the sine series coefficients function of f_k.

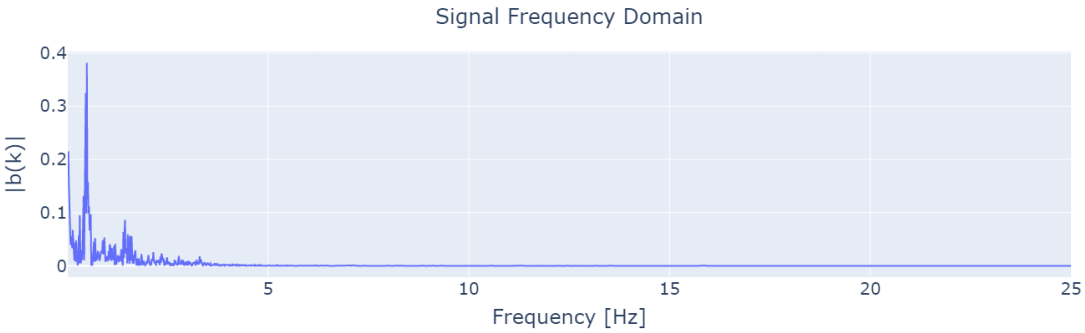

Figure A.3: Signal in the frequency domain